Ocean productivity in the Gulf of Cadiz over the last 50 kyr

Penaud A.[(a)], Eynaud F.[(b)], Etourneau J. [(b,c)], Bonnin J.[(b)], de Vernal A. [(d)], Zaragosi S.[(b)], Kim J.-H. [(e)], Kang S. [(f)], Gal, J.-K [(e)], Oliveira D. [(g,h)], Waelbroeck C. [(i)]

(a) *University Brest, CNRS, Ifremer, Geo-Ocean UMR 6538, Plouzane, France*

(b) *University Bordeaux, CNRS, EPOC, Pessac, France*

(c) *EPHE/PSL Research University, Paris, France*

(d) *Geotop, Université du Québec à Montréal (UQAM), Montréal, QC, Canada*

(e) *KOPRI Korea Polar Research Institute, Incheon, South Korea*

(f) *Hanyang University ERICA, Gyeonggi-do, South Korea*

(g) *CCMAR, Centro de Ciências do Mar, Universidade do Algarve, Campus de Gambelas, Faro, Portugal*

(h) *Divisão de Geologia e Georecursos Marinhos, Instituto Português do Mar e da Atmosfera (IPMA), Algés, Portugal,*

(i) *LOCEAN/IPSL, Sorbonne Université-CNRS-IRD-MNHN, Paris, France*

*Corresponding author. Tel.: +33-298-498-741; fax: +33-298-498-760.

E-mail address: aurelie.penaud@univ-brest.fr.

Highlights

- Productivity (PP) in the Gulf of Cadiz is dependent on the seasonality control for both upwelling and nutrient-enriched freshwater inputs.
- We show generally high PP, carbon export, and remineralisation during the last glacial period at the study site.
- The Last Glacial Maximum had lower $\Delta\delta^{13}C$ than the Heinrich Stadials with sustained high PP likely allowing enhanced carbon sequestration.

Abstract

Reconstructions of ocean primary productivity (PP) help to explain past and present biogeochemical cycles and climate changes in the oceans. We document PP variations over the last 50 kyr in a currently oligotrophic subtropical region, the Gulf of Cadiz. Data combine refined results from previous investigations on dinocyst assemblages, alkenones, and stable isotopes (^{18}O, ^{13}C) in planktonic (*Globigerina bulloides*) and endobenthic (*Uvigerina mediterranea*) foraminifera from cores MD04-2805 CQ and MD99-2339, with new isotopic measurements on epibenthic (*Cibicides pachyderma–Cibicidoides wuellerstorfi*) foraminifera and dinocyst-based estimates of PP using the new n = 1,968 modern database. We constrain PP variations and export production by integrating qualitative information from bio-indicators with dinocyst-based quantitative reconstructions such as PP and seasonal sea-surface temperature and information about remineralization from the benthic $\Delta\delta^{13}C$ (difference between epi- and endo-benthic foraminiferal $\delta^{13}C$ signatures). This study also includes new information on alkenone-based SST and total organic carbon which provides insights into the relationship between past regional hydrological activity and PP regime change. We show that PP, carbon export, and remineralization were generally high in the NE subtropical Atlantic Ocean during the last glacial period and that the Last Glacial Maximum (LGM) had lower $\Delta\delta^{13}C$ than the Heinrich Stadials with sustained high PP, likely allowing enhanced carbon sequestration. We link these PP periods to the dynamics of upwelling, active almost year-round during stadials, but restricted to spring-summer during interstadials and LGM, like today. During interstadials, nutrient advection through freshwater inputs during autumn–winter needs also to be considered to fully understand PP regimes.

Keywords: Dinocysts; Stable isotopes; Alkenones; Last Glacial Maximum; Heinrich Stadials; Primary productivity; Remineralization

1. Introduction

Reconstructing primary productivity (PP) in the past surface ocean is a challenging topic to address in paleoceanography given the limited number of proxies that can be used up to date (e.g. biogenic opal fluxes or mass accumulation rates of total organic carbon). Nevertheless, some bioindicators like dinocysts can offer an alternative and useful way when targeting specific fractions that reach the seabed and are preserved in marine sediments, such as those associated with dinoflagellate production (Radi & de Vernal, 2008). Establishing a strong relationship between PP and dinocyst assemblages could, therefore, significantly improve the quantification of past PP in numerous key oceanographic settings. This is what we have undertaken in the Gulf of Cadiz (GoC), located in the northeastern (NE) subtropical Atlantic, based on the modern analogue technique (MAT). Indeed, this region, part of an Eastern Boundary Current (EBC) system characterized by high annual and seasonal marine PP (e.g. Hagen, 2001), is particularly interesting for studying i) the PP-derived organic matter export toward the seafloor and ii) its potential influence on the biological pump. Moreover, the GoC is considered as an exceptional region for evaluating past PP during contrasted climatic periods as well as for testing different methodological approaches, since it is characterized by pronounced shifts in latitudinal fronts associated with abrupt climate changes.

Apart from abiotic processes, CO_2 storage evolution is governed by continental and marine primary producers through biological carbon fixation, export, and burial. Today, the GoC is characterized by an oligotrophic regime associated with low CO_2 storage (Huertas et al., 2006, 2009; Flecha et al., 2012) and nutrient-poor waters carried by the Azores Current and surface Atlantic waters (i.e. between the surface and around 100 m depth) into the GoC. However, this oligotrophic zone experienced a different PP regime during the last glacial period, characterized by overall higher PP (Wienberg et al., 2010), especially across the stadials (Penaud et al., 2011, 2016), caused by changes in the upwelling dynamics. Over the last 50 kyr, from the subtropical to the NE North Atlantic Ocean (including Irish-Norwegian seas), long-term northward migration of cold-water corals and thus of high PP centers also occurred, as previously documented (Freiwald et al., 2004; Dorschel et al., 2005; Rüggeberg et al., 2007; Eisele et al., 2008; Frank et al., 2005, 2009; de Haas et al., 2009; Wienberg et al., 2009, 2010), with interglacial (glacial) obliquity maxima favoring phytoplanktonic growth in northern (southern) North Atlantic latitudes (Wienberg et al., 2010; Penaud et al., 2016). Enhanced glacial PP was also noted off Mauritania, one of the major upwelling areas of the world ocean (Eisele et al., 2011; McKay et al., 2014), with generally cold-water coral growth restricted to glacial and stadial periods at low latitudes (17°N).

Because there are still large uncertainties surrounding the evolution of PP in the NE Atlantic subtropical region, it is important to investigate this further in strategically located regions such as the GoC. This can be done by comparing existing and new proxy records. Here, we combine new dinocyst-based PP estimates in the GoC, derived from MAT calculations thanks to an updated database of n = 1,968 modern analogues (de Vernal et al., 2020), to a set of geochemical proxies. The latter includes Total Organic Carbon (TOC) content and indirect signals reconstructed from the difference between epi- and endo-benthic foraminiferal $\delta^{13}C$ signatures (benthic $\Delta^{13}C$), to better account for past changes in the carbon cycle at a regional scale, from productivity export to sequestration *versus* remineralization.

2. Material and methods

Two marine cores are the basis of this study. The MD04-2805 CQ core (southern GoC; 34.52°N; 7.02°W; 859 m deep; Figure 1a) was retrieved from the Moroccan margin, in a location now under the influence of the Portugal-Canary Eastern Boundary Current (EBC) upwelling system. Today, this seasonal upwelling system is mainly active in summer (from late May to early October; Aristegui et al., 2005) due to the seasonal migration of the Azores High coupled with the Inter Tropical Convergence Zone dynamics (Fiúza et al., 1998), with variable extents of upwelling filaments (e.g. Wooster et al., 1976; Peliz et al., 2005; Garcia Lafuente et al., 2006; Garcia Lafuente & Ruiz, 2007). The MD99-2339 core was collected in the central sector of the GoC (35.89°N; 7.53°W; 1,170 m deep; Figure 1a) within a contouritic field (Habgood et al., 2003). The GoC is under the influence of river discharges such as the Guadalquivir River, one of the largest rivers in Spain, whose turbidity plumes in autumn–winter (i.e. at times of higher rainfall) are crucial for phytoplankton blooms during the subsequent spring–summer seasons (Garcia Lafuente & Ruiz, 2007; Caballero et al., 2014). Fluvial inputs from major rivers such as the Guadalete, Guadania, and Tinto-Odiel also contribute to high turbidity levels on the continental shelf of the GoC (Navarro et al., 2012) and to high biological productivity in the eastern GoC (Prieto et al., 2009).

2.1. New MD04-2805 CQ and MD99-2339 chronologies

2.1.1. MD04-2805 CQ chronology

In addition to six existing ^{14}C dates from mollusk shells (Penaud et al., 2010), eight new ^{14}C dates were obtained from planktonic foraminiferal samples (Table S1; cf. section "7. Data availability"). The new dates, together with data from SST proxies (dinocyst- and alkenone-based) and benthic and planktonic foraminiferal isotopes, indicate re-sedimentation or mud-flow issues from 140–147 cm to 270–287 cm that were not identified in Penaud et al. (2010). A detailed analysis of the X-ray radiography (SCOPIX, EPOC laboratory) of core MD04-2805 CQ revealed the existence of micro faults between 160 and 166 cm and between 263 and 285 cm, within a clayey-silty sedimentary matrix (Figure 1d).

These facies, within "section 2" of the core, are unique in the whole 7.72-m long core. They were observed on thin sections examined under a transmitted polarizing microscope for micro-facies and structure description (Figure 1d). Inverted ages and micro-faults led us to adopt a conservative approach and discard data from 300 to 140 cm (i.e. three new ^{14}C dates rejected). Moreover, we added a supplementary age constraint with respect to the age model entirely based on calibrated ^{14}C

ages as published in Waelbroeck et al. (2019), taking advantage of the large amplitude (planktonic foraminiferal-based) SST signals reconstructed in both MD04-2805Q and MD99-2339 cores (Penaud et al., 2011), in which the HS1-BA transition is easily recognizable (Figure S1; cf. section "7. Data availability"). This led us to assign an age of 14.64 ± 0.15 cal ka BP (after the Greenland Ice Core Chronology GICC05, Rasmussen et al., 2014) at 140 ± 8 cm (Table S1; cf. section "7. Data availability"), thereby defining a new robust chronological marker resulting in an improved age model.

The age–depth relationship of core MD04-2805 CQ was built accounting for both the age and depth uncertainties in the 11 retained ^{14}C dates and 1 additional chronological marker, using the age–depth modeling routine "Undatable" (Lougheed & Obrochta, 2019) (Figure 1c). For continuity between this work and previous studies (Penaud et al., 2010, 2011), results obtained in the 140–300 cm interval are shown in the result section with reference to depth (Figures 2 and 3) and are not subsequently addressed in the discussion, in which data are presented *versus* age cal ka BP.

2.1.2. MD99-2339 chronology

The age model of core MD99-2339 was not included in the dataset of Waelbroeck et al. (2019) because its age model could not be entirely based on MD99-2339 records but had to be partly derived from an alignment to core MD04-2805Q, thereby introducing additional dating uncertainties. The chronology of core MD99-2339 we adopted was established as follows: i) the ages in the interval spanning 0–11 ka BP were based on six previously published ^{14}C dates from planktonic foraminifera (Voelker et al., 2006), ii) the chronology of the 11–26 ka BP interval was defined based on the alignment of the *Globigerina bulloides* $\delta^{18}O$ and SST variations with those of the nearby core MD04-2805 CQ (10 tie points), and iii) the chronology of the 26–49 ka BP interval was based on the alignment of the *Globigerina bulloides* $\delta^{18}O$ and SST variations with the NGRIP $\delta^{18}O$ data (12 tie-points) as described in Penaud et al. (2016) (Table S2; cf. section "7. Data availability").

In the same way as for core MD04-2805 CQ, the age–depth relationship of core MD99-2339 was built accounting for both age and depth uncertainties of the ^{14}C dates and chronological markers, using the age-depth modeling routine "Undatable" (Lougheed & Obrochta, 2019) (Figure 1b).

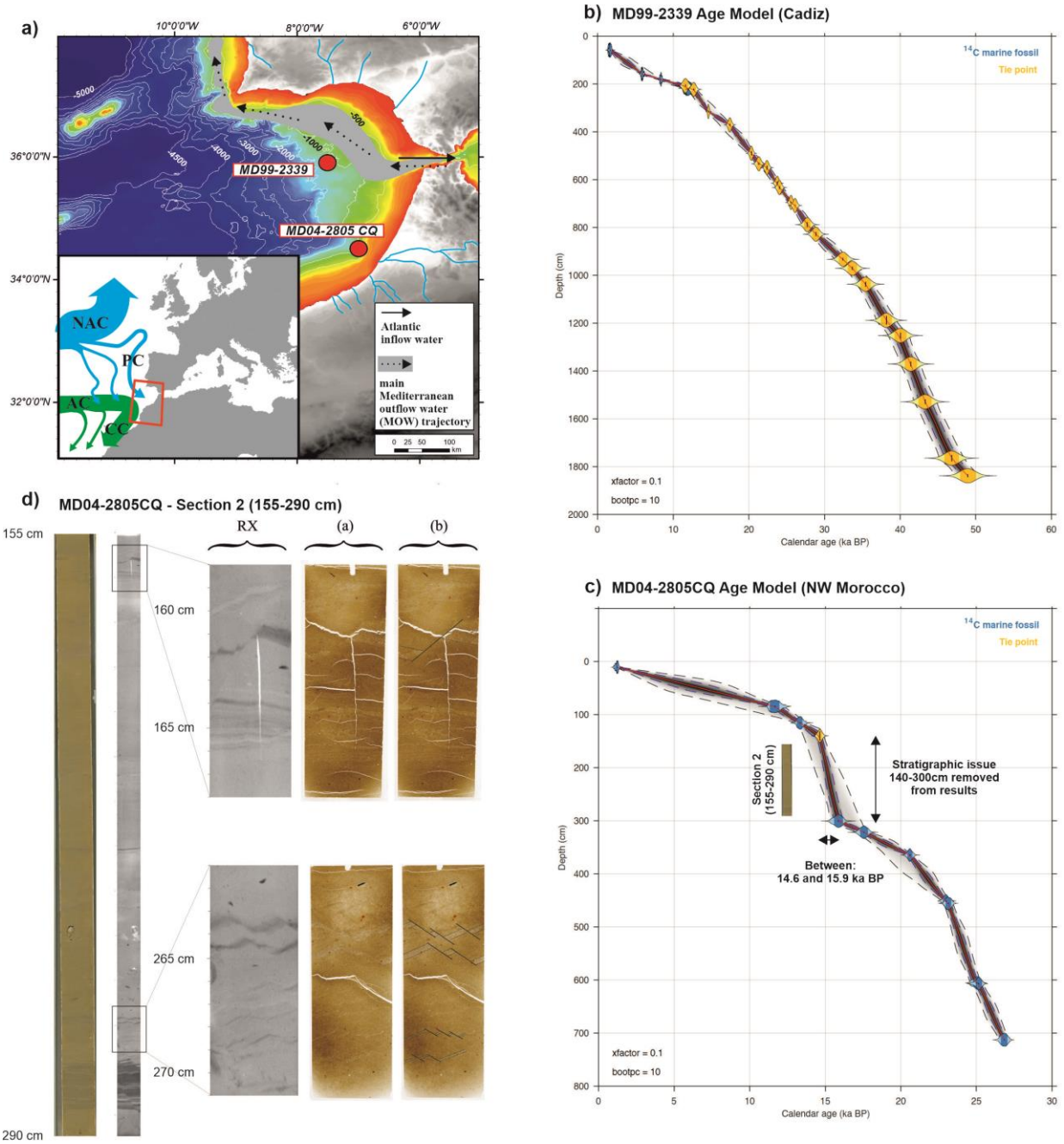

Figure 1: a) *Area of interest with major sea-surface features. Study cores MD04-2805 CQ and MD99-2339 are indicated on the large map, also depicting the bathymetry of the study area. The small map on the left present large scale North Atlantic currents with: the North Atlantic Current (NAC), the Portugal Current (PC) flowing southward from 45°N to 30°N, the Azores Current (AC) derived from the southern branch of the Gulf Stream and flowing eastward to the Gulf of Cadiz at about 35°N, and the Canary Current (CC) fed by both the AC and the PC. Together, these currents form the Eastern Boundary Current of the North Atlantic subtropical gyre.* ***b)*** *MD99-2339 age model : 6* ^{14}*C dates on the 0-11 ka BP interval (cf. Voelker et al., 2006), 10 tie-points on the 11-26 ka BP interval (alignment of Globigerina bulloides* $\delta^{18}O$ *and SST signals of core MD99-2339 with*

those of core MD04-2805 CQ), 12 tie-points mainly on the 26-49 ka BP interval (alignment of G. bulloides $\delta^{18}O$ and SST signals with NGRIP $\delta^{18}O$ data as in Penaud et al., 2016). Age-depth relationship built using the age-depth modelling routine "Undatable" (Lougheed and Obrochta, 2019). ***c)*** *MD04-2805 CQ age model: six ^{14}C dates on bivalves (Penaud et al., 2010) combined with 8 new ^{14}C dates from planktonic foraminifera. One more age constraint (tie point) is based on the calibrated ^{14}C ages of consistently dated Atlantic sediment cores by Waelbroeck et al. (2019). Interval 140-300 cm discarded (inverted dates and micro-faulted levels unique in the 7.72 m long core within a clayey-silty sedimentary matrix). Age model built using the age-depth modelling routine "Undatable" (Lougheed and Obrochta, 2019).* ***d)*** *MD04-2805 CQ "section 2" (155-290 cm). From the left to the right: photography of section 2 affected by micro faults that are revealed by radiography RX: zooms of RX and photographs of two thin indurated slides (a) and schematic representation of some of the micro-faulted structures (b).*

2.2. MD04-2805 CQ stable isotopic analyses

Measurements of stable isotopes ($\delta^{18}O$ and $\delta^{13}C$) in planktonic (*Globigerina bulloides*; 76 samples) and endobenthic (*Uvigerina mediterranea*; 77 samples) foraminifera were obtained at the LSCE (Gif-sur-Yvette, France) and University of Bordeaux (UMR 5805 EPOC, France), respectively, from the 250–315 µm size fraction at every 10 cm (Penaud et al., 2010).

In this study, additional data on the epifaunal benthic foraminifera (handpicked from the > 150 µm size fraction, 98 samples) were obtained to document the isotopic composition of bottom waters at the study site. In most of the levels, the only recovered species was *Cibicides pachyderma*. Since we did not observe any significant differences between the isotopic values of *Cibicidoides* (syn. *Planulina*) *wuellerstorfi* and *C. pachyderma* in samples in which they co-occurred, either of these two species was used for epibenthic stable isotope analysis.

The $\delta^{18}O$ and $\delta^{13}C$ *versus* VPDB (Vienna PDB) were measured on an Isoprime 100 mass spectrometer on samples of 1–4 specimens. The VPDB was defined based on the NBS19 calcite standard ($\delta^{18}O$ = 2.20% and $\delta^{13}C$ = +1.95%) (Coplen, 1988). The mean reproducibility (1σ) of carbonate standards was ± 0.05 ‰ for $\delta^{18}O$ and ± 0.03 ‰ for $\delta^{13}C$. The measured NBS18 $\delta^{18}O$ was -23.27 ± 0.10 ‰ and $\delta^{13}C$ is -5.01 ± 0.03 ‰.

2.3. MD04-2805 CQ dinocyst data

2.3.1. New dinocyst-based environmental parameter quantifications

MAT was run on "R" version 3.6.3 to the dinocyst assemblages of cores MD04-2805 CQ (Penaud et al., 2010) and MD99-2339 (Penaud et al., 2016), after log transformation of taxa percentages. The MAT compares fossil records with modern dinocyst assemblages from the most up-to-date version of the standardized "modern" Northern Hemisphere dinocyst database, which includes the abundance of 71 taxa and 1,968 sites in relation to 17 modern environmental parameters (de Vernal et al., 2020). This method relies on the assumption that modern relationships between environmental parameters and dinocyst assemblages were the same in the past (e.g. Guiot & de Vernal, 2007). Uncertainties may, however, arise from the probable lack of modern analogues corresponding to fossil assemblages (e.g. Guiot & de Vernal, 2007; de Vernal et al., 2020). The quantification of environmental parameters is based on a weighted average of the values obtained for a maximum of the five best modern analogues, with the maximum weight being given to the closest ones. The closest analogue is characterized by a similarity distance referred to as the minimal distance (Dmin). The threshold distance for analogues to be considered significant is around 1.3 ($d_T = 1.3$). Hence, we may define analogues as: i) "good" when the distance (d) < $d_T/2$, ii) "acceptable" when $d_T/2 < d < d_T$, or iii) "poor" when $d > d_T$ (de Vernal et al., 2005). If Dmin is higher than d_T, this consists in a non-analogue configuration with no quantifications. Here are shown reconstructions for summer and winter SST and salinity (SSS), and annual PP. The uncertainty defined from the root mean square error (RMSE or standard deviation of the mean residuals) was ± 1.7°C and ± 1.2°C for SST_{summer} and SST_{winter} respectively, ± 2.0 psu and ± 1.0 psu for SSS_{summer} and $SSS_{winter,}$ respectively, and ± 138 gC m^{-2} for PP_{annual}. We also calculated the difference between summer and winter SST in order to document the seasonal differences in temperature (SST seasonality). Furthermore, the enlarged n = 1,968 dinocyst database includes additional sites from middle and low latitudes and provides additional environmental parameters: seasonal PP with strong correlations between all PP parameters (de Vernal et al., 2020) for winter (RMSE : 250 µgC m^{-2} day^{-1}), spring (RMSE : 542 µgC m^{-2} day^{-1}), summer (RMSE : 720 µgC m^{-2} day^{-1}) and fall (RMSE : 240 µgC m^{-2} day^{-1}); mean annual and winter PP being the best reconstructed. Although seasonal and annual PP parameters are not independent, we used them as proxies for the overall PP and indicators for the annual PP cycle. The updated n = 1,968 also includes the "distance to the coast" parameter, which shows correlations with the bathymetry and explains part of the variance in the distribution of dinocyst assemblages. We used this parameter (expressed in degrees) as an index of coastal proximity (i.e. inshore *versus* offshore assemblages).

2.3.2. Canonical Correspondence Analysis (CCA)

Multivariate analyses were performed with Past software version 1.75b (Hammer et al., 2001). Canonical Correspondence Analysis (CCA) was applied to the dinocyst assemblages (expressed in percentages and absolute concentrations with no transformation) of core MD04-2805 CQ to capture the main factors (i.e. environmental variables including stable isotope data, alkenone-based SST, and dinocyst-based quantifications) that could typify the control of PP in the study area.

2.4. MD99-2339 Total Organic Carbon and alkenone-based SST

Total organic carbon (TOC; in %) was assessed at the University of Bordeaux (UMR 5805 EPOC, France). Measurements were done on 50 samples and performed by the total combustion of homogenized sediment samples using a LECO C-S 125 analyzer after treatment of the sediment with hydrochloric acid (1N) to remove calcium carbonate. Precision of TOC measurements from standard and sample replicates was higher than ± 0.5%.

Total lipids were extracted at the University of Bordeaux (UMR 5805 EPOC, France). Extracts were obtained from 70 freeze-dried and homogenized sediment samples (15–20 g) using a mixture of 9 mL dichloromethane/methanol (3:1; v:v) following several steps of sonication and centrifugation until all organic compounds had been properly extracted. After drying with N_2 at +35°C, the alkenones were separated from the other organic compounds on a Al_2O_3 column using hexane/dichloromethane (1:1; v:v). These were then analyzed at the University of Hanyang, South Korea, where they were co-injected with a hexatriacontane standard before assessment on a Shimazu GC (Shimazu Corporation, Kyoto, Japan) fitted with a flame ion detector (FID) with a DB–5 column (60 m × 0.25 mm, 0.25 μm, Agilent). The $U^{k'}_{37}$ index (Prahl & Wakeham, 1987) was calculated as the ratio between the different $C_{37:2}$ and $C_{37:3}$ areas, and annual mean SSTs were computed using the equation of Müller et al. (1998), with a standard error of about 1.5°C.

3. Results

The link to the new results presented in this section can be found in section 8 “Data availability” (Tables S1 and S2).

3.1. Benthic isotopic data of core MD04-2805 CQ

In this study, *C. pachyderma–C. wuellerstorfi* $\delta^{18}O$ values range between 1.5 and 3.5 ‰ (Figure 2). They show relatively constant values averaging 3.3 ‰ in the lower part of the core, up to 300 cm, followed by a gradual decrease to mean values of 1.8 ‰ in the 80–0 cm interval, similarly to the *U. mediterranea* $\delta^{18}O$ (Penaud et al., 2010).

Epifaunal *C. pachyderma–C. wuellerstorfi* have been shown to record the $\delta^{13}C$ of ambient bottom-water dissolved inorganic carbon (DIC) with minor isotopic fractionation (Duplessy et al., 1984; Zahn et al., 1986; Gottschalk et al., 2016a; Schmittner et al., 2017), even in eutrophic areas (Eberwein & Mackensen, 2006). Here, the epibenthic $\delta^{13}C$ values can be seen to range between 0.1 and 1.5‰ (mean of 0.9) (Figure 2). In addition, the shallow infaunal *U. mediterranea* $\delta^{13}C$ (Figure 2) reflects the $\delta^{13}C$ of pore waters, which depends on the export flux of organic matter and availability of dissolved oxygen in bottom waters (e.g. McCorkle et al., 1990; Mackensen & Licari, 2003; Fontanier et al., 2006). The amount of sedimentary organic carbon respiration or remineralization can be captured by the difference in $\delta^{13}C$ between bottom waters and pore waters (Gottschalk et al., 2016a; Hoogakker et al., 2015). Thus, we used the *C. pachyderma–C. wuellerstorfi versus U. mediterranea* $\delta^{13}C$ signal (benthic $\Delta\delta^{13}C$) as a proxy for remineralization in the sediments. Since both benthic isotopic datasets were not acquired at the same levels, the measured *C. pachyderma–C. wuellerstorfi* $\delta^{13}C$ were interpolated to obtain *C. pachyderma–C. wuellerstorfi* $\delta^{13}C$ values at the same depths as the *U. mediterranea* measurement depths (grey filling on Figure 2), and vice versa (black line in Figure 2). In core MD04-2805 CQ, benthic $\Delta\delta^{13}C$ values range between 0.2 and 2.2‰ (Figure 2). The benthic $\Delta\delta^{13}C$ peaks (i.e. red dotted horizontal lines in Figure 2) are mainly explained by depleted endobenthic $\delta^{13}C$ (*U. mediterranea*) values. These peaks generally correspond to heavier planktonic $\delta^{13}C$ and $\delta^{18}O$ values (*Globigerina bulloides*), thus suggesting higher PP and low SSTs.

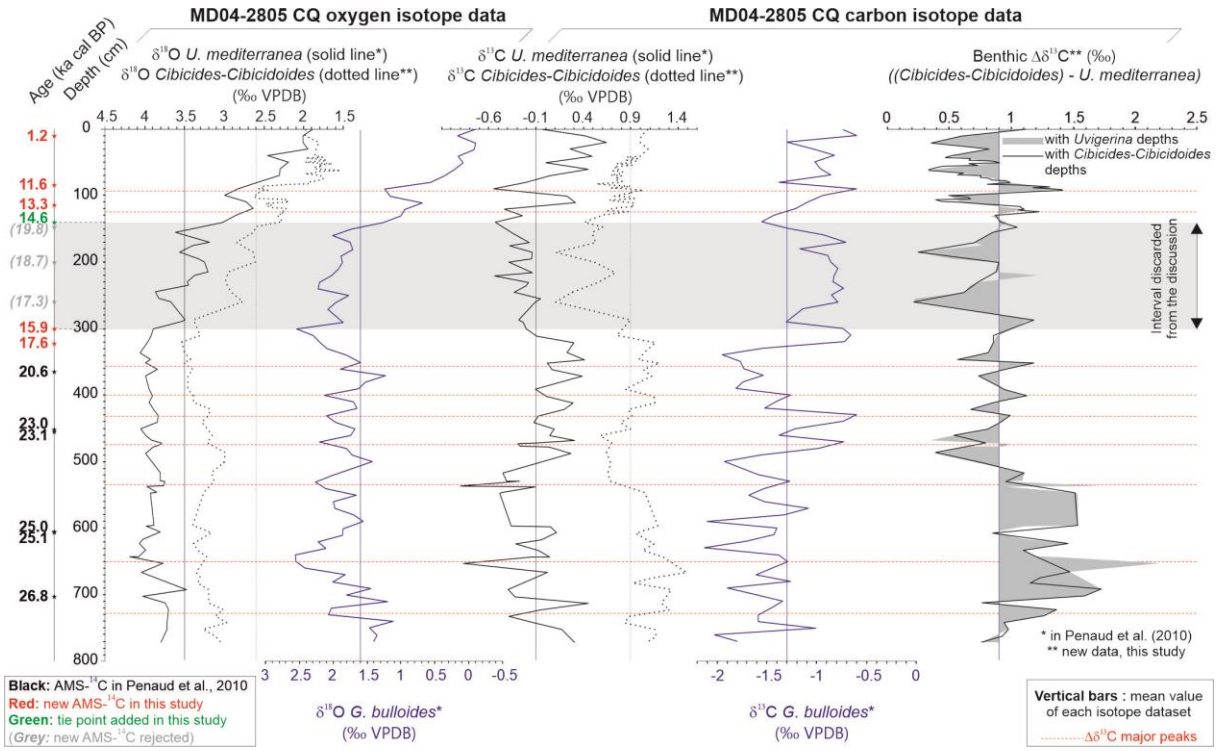

Figure 2: *Core MD04-2805 CQ. Core depths are displayed in centimetres and in ages (ages indicated on the scale correspond to the pointers used to establish the stratigraphy of the core) along the vertical axis. Stable isotope ($\delta^{18}O$ and $\delta^{13}C$) data are displayed for planktonic (Globigerina bulloides with blue lines) and benthic foraminifera (Uvigerina mediterranea with black solid lines, and Cibicides pachyderma–Cibicidoides wuellerstorfi with black dotted lines). For the calculation of the benthic $\delta^{13}C$ gradient ($\Delta\delta^{13}C$) (C. pachyderma–C. wuellerstorfi - U. mediterranea), the measured Cibicidoides spp. $\delta^{13}C$ values were interpolated to obtain C. pachyderma–C. wuellerstorfi $\delta^{13}C$ values at the same depths as the U. mediterranea measurement depths (grey filling), and vice versa (black line). Red dotted lines highlight major peaks of $\Delta\delta^{13}C$ representing higher organic remineralisation in bottom sediments at the study site.*

3.2. Sea-surface parameter estimates based on the n = 1,968 dinocyst database

Dinocyst-derived environmental parameters were obtained from dinocyst assemblages of cores MD04-2805 CQ and MD99-2339. For unedited comparison and discussion, we decided to use calculated parameters with both the n = 1,492 (already published) and n = 1,968 databases (Figure 3). In core MD04-2805 CQ, 15 of 80 spectra did not yield estimates with the n = 1,492 database because of the lack of modern analogues, but the number of levels having no analogues decreased to 11 using the n = 1,968 database. Similarly, in core MD99-2339, 6 of 158 spectra had no modern

analogues using the n = 1,492 database, whereas all levels yielded estimates with the updated n = 1,968 database. Moreover, the number of analogues for each level was significantly higher with the updated modern dinocyst database (Figure 3). Overall, most of the estimates are "acceptable", with the distance of best analogues ranging between 0.6 and the threshold distance (d_T = 1.3 for the n = 1,968 database and d_T = 1.4 for the n = 1,492 database). Holocene samples with modern analogues close to the study cores yielded "good" results with Dmin < d_T (Figure 3).

The closest analogues in the n = 1,968 modern dinocyst database are mainly from the GoC, Bay of Biscay, North Sea, Cap Verde, Gulf of Guinea, and Gulf of Mexico (dots in Figure 4 with labels as in de Vernal et al., 2020 for all closest analogues found for both study cores). We attributed seven code colors for the closest analogues illustrated on Dmin (Figure 3) in order to show the areas where the modern analogues yielding peaks of high PP_{annual} values came from (dotted lines in Figure 3). Downcore, over the last 27 kyr, peaks of high PP_{annual} (>500 gC m^{-2}) in core MD04-2805 CQ mainly correspond to analogues from the Gulf of Guinea, while the peaks of extremely high PP_{annual} (>1,000 gC m^{-2}) in core MD99-2339 between 27 and 50 ka BP correspond to analogues from the Gulf of Mexico. Peaks of high PP were also recorded with the n = 1,492 dataset, but their amplitudes were much larger with the additional sites of the updated n = 1,968 database. Moreover, while the SSS and SST profiles from core MD99-2339 were generally flat with the n = 1,492 dataset, with the exception of cold pulses during stadials, the n = 1,968 database allowed a much improved capture of variability. The SST and SSS minima show similar values with the two dinocyst datasets but show larger variability and amplitudes between the stadials with the new n = 1,968 database. In core MD04-2805 CQ, the new estimates suggest that SSS_{winter} varied mostly between 31.3 and 36.4 psu, with Holocene values of about 36 psu. They also indicate SST_{winter} variation between +3.4 and +28.7°C with Holocene values of about +15.9°C. In core MD99-2339, the new estimates put SSS_{winter} between 28.9 and 36.2 psu, with Holocene values of about 35.9 psu, and SST_{winter} between +3.3 and +28.6°C with Holocene values of about +16.7°C. For both cores, Holocene SSS and SST estimates fall within the modern winter–summer seasonal range (Figure 3).

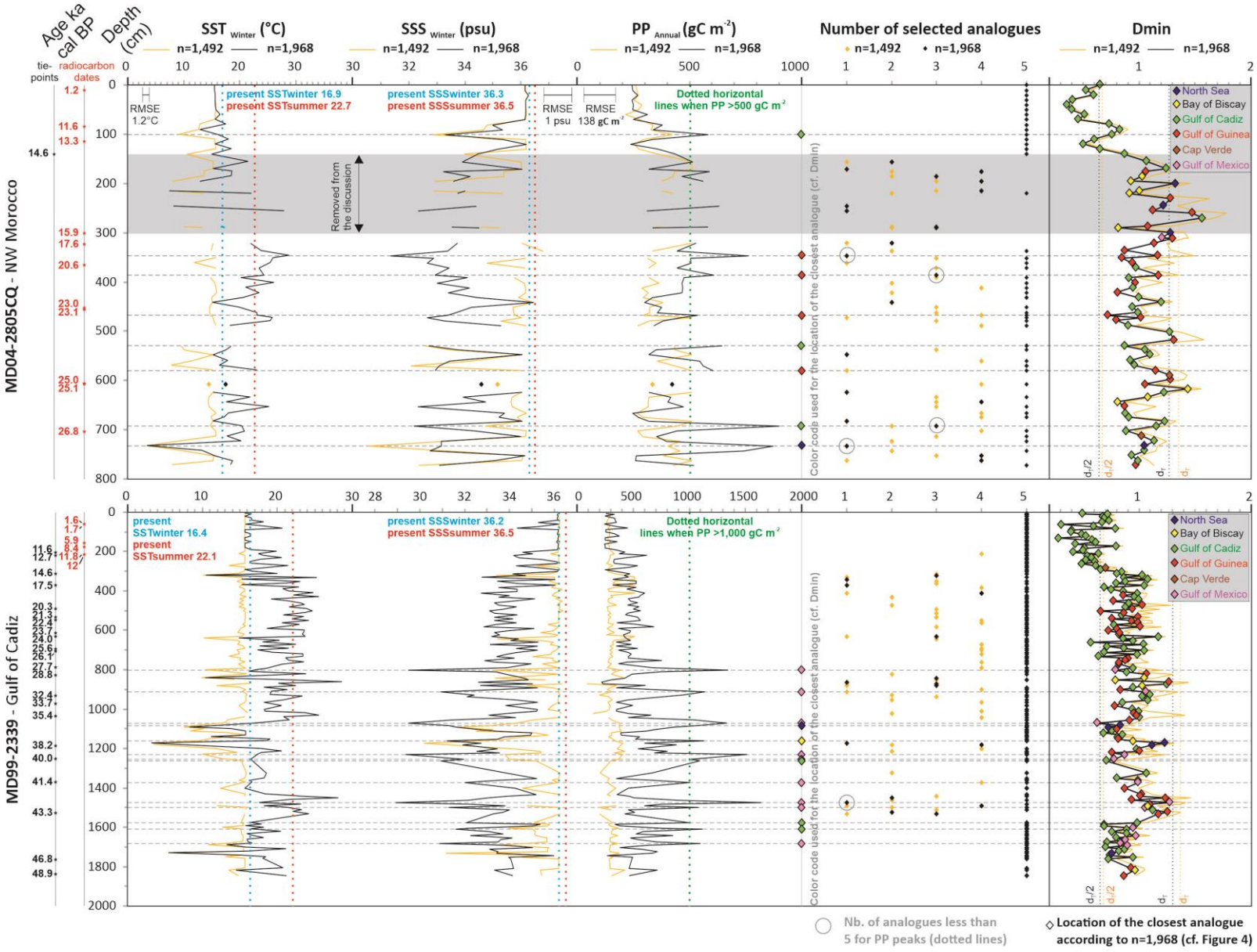
Age ka cal BP
Depth (cm)
tie-points
radiocarbon dates
SST Winter (°C)
SSS Winter (psu)
PP Annual (gC m-2)
Number of selected analogues
Dmin
n=1,492
n=1,968
MD04-2805CQ - NW Morocco
RMSE 1.2°C
present SSTwinter 16.9
present SSTsummer 22.7
present SSSwinter 36.3
present SSSsummer 36.5
RMSE 1 psu
RMSE 138 gC m-2
Dotted horizontal lines when PP >500 gC m-2
Removed from the discussion
Color code used for the location of the closest analogue (cf. Dmin)
North Sea
Bay of Biscay
Gulf of Cadiz
Gulf of Guinea
Cap Verde
Gulf of Mexico
MD99-2339 - Gulf of Cadiz
present SSTwinter 16.4
present SSTsummer 22.1
present SSSwinter 36.2
present SSSsummer 36.5
Dotted horizontal lines when PP >1,000 gC m-2
Nb. of analogues less than 5 for PP peaks (dotted lines)
Location of the closest analogue according to n=1,968 (cf. Figure 4)

Figure 3: *Cores MD04-2805 CQ and MD99-2339 with vertical scales in depth (cm) and stratigraphic pointers used for the establishment of both age models (radiocarbon dates identified in red and other tie points identified in black; e.g. MD04-2805 CQ: stratigraphic pointers consist in 11 retained ^{14}C dates and one tie point, cf. Figure 2). Selected environmental parameters are highlighted with both dinocyst databases for comparison: n=1,492 (de Vernal et al., 2013) in orange, and n=1,968 (de Vernal et al., 2020) in black. SST: Sea Surface Temperature. SSS: Sea Surface Salinity. PP: Primary Productivity. The number of retained modern analogues is shown for each dinocyst-based quantifications, as well as the statistical distance of the best retained analogue for each analysed sample (i.e. Dmin). Dmin is represented with continuous lines, then allowing to highlight all analysed samples. The closest analogue found with the n=1,968 database is represented by a colored diamond (cf. legend in the Figure), this color code referring to the areas highlighted in maps of Figure 4. It is worth noting that SST-SSS-PP curves have been interrupted in case of non-analogue configuration (i.e. if the threshold of Dmin is exceeded). This representation highlights the importance of intervals with or without quantifications. If SST-SSS-PP curves are continuous, then all samples analysed along the curves have quantifications. Diamond symbols used for one level of core MD04-2805 CQ highlight quantifications succeeded in a non-analogue configuration interval centered on 600 cm. Dotted horizontal lines underline intervals of high dinocyst-based PP estimates. Present-day seasonal values for SSTs and SSSs are provided for each core location with blue and red dotted vertical lines.*

3.3. Total Organic Carbon and alkenone based SST in core MD99-2339

In core MD99-2339, the TOC ranges from 0.3 to 1.2 % (mean value of 0.5 %) with the higher values comprised between 15 and 27 ka BP (Figure 6). Also, our new alkenone-based SST record provides strikingly similar amplitude and SST values to those generated from core MD04-2805 CQ (Penaud et al., 2010), with colder temperatures (+8.1°C) during the glacial period and the warmest ones during the Holocene interval (+20.3°C; Figure 5). We compare these new data with the other records acquired for both cores below in the discussion (section 4.1).

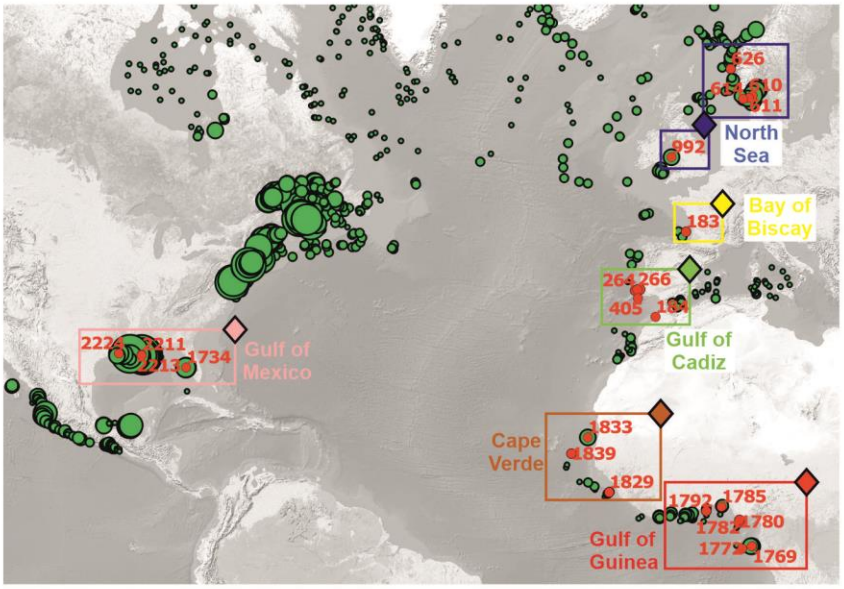

PP $_{Annual}$ (gC m^{-2})

- Selected analogs

Database n=1968

- 25 - 224
- 224 - 423
- 423 - 622
- 622 - 820
- 820 - 1019
- 1019 - 1218
- 1218 - 1417
- 1417 - 1616
- 1616 - 1815
- 1815 - 2014

◇ **Color code for provinces where Dmin are calculated: closest analogues (Figure 3)**

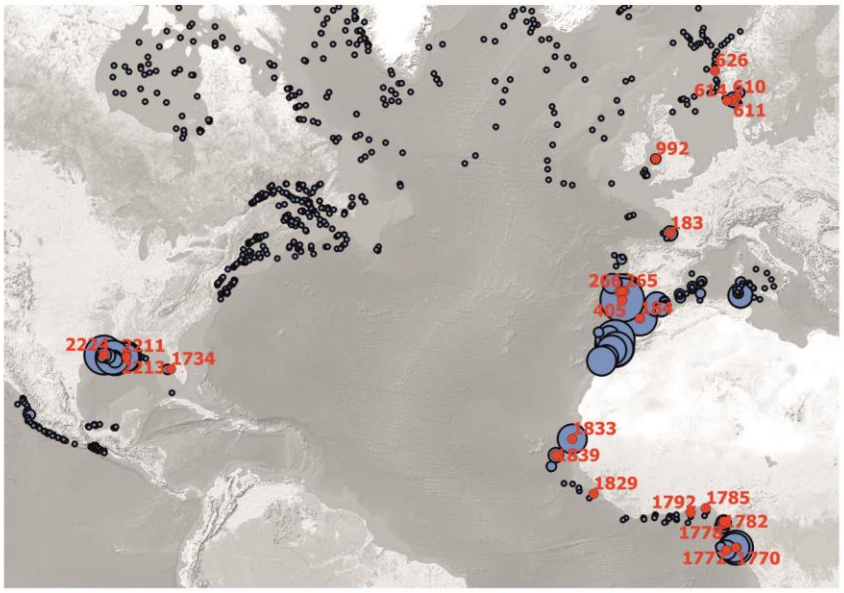

L. machaerophorum (%)

- Selected analogs

Database n=1968

- 0 - 10
- 10 - 20
- 20 - 30
- 30 - 40
- 40 - 50
- 50 - 60
- 60 - 70
- 70 - 80
- 80 - 90
- 90 - 100

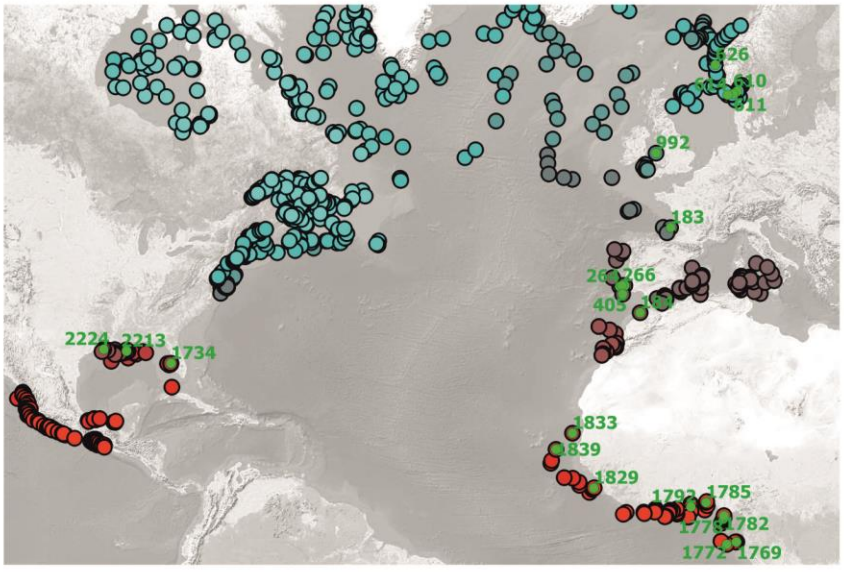

SST $_{Winter}$ (°C)

- Selected analogs

Database n=1968

- -1,9 - 1,2
- 1,2 - 4,3
- 4,3 - 7,4
- 7,4 - 10,4
- 10,4 - 13,5
- 13,5 - 16,6
- 16,6 - 19,7
- 19,7 - 22,8
- 22,8 - 25,8
- 25,8 - 28,9

Figure 4: *Maps established with QGis with the points encompassing the n=1,968 modern dinocyst database (de Vernal et al., 2020). From top to bottom:* PP_{annual} *for annual Primary Productivity, Lingulodinium machaerophorum percentages,* SST_{winter} *for winter Sea Surface Temperature. Colored dots with labels (dots and numbers in reds for the two upper maps, and in green for the bottom map) are as in de Vernal et al. (2020) and highlight all closest analogues found for dinocyst-based quantifications performed on both study cores (MD04-2805 CQ and MD99-2339).*

4. MD04-2805 CQ core: Paleoenvironmental changes over the last 27 kyr in the Subtropical NE Atlantic Ocean

4.1. SST and SSS variations

4.1.1. Holocene reconstructions

The new dinocyst-based SST (Figure 5d) and SSS (Figure 5f) estimates from cores MD04-2805 CQ and MD99-2339 show similar stable patterns, thereby confirming regionally consistent hydrological sea-surface conditions in the central and southern GoC (Penaud et al., 2011, 2016). Moreover, the dinocyst-derived qualitative paleothermometer index (Warm vs. Cold (W/C) dinocyst ratio according to Penaud et al., 2016; Figure 5c) generally matches the $\delta^{18}O$ signal in both cores (Figure 5b), thus strengthening the robustness of dinocyst assemblages for capturing sea-surface hydrological conditions in the subtropical NE Atlantic Ocean (Penaud et al., 2011, 2016). Mean dinocyst-derived SSTs of +21°C in summer (not shown) and +16°C in winter during the Holocene sections of both studied cores are close to present-day SSTs (+22.4°C: red star and +16.6°C: blue star, respectively, on Figure 5d), with modern analogues found close to the study site (Figures 3 and 4). In comparison, alkenone-based SSTs exhibit mean annual values of +19°C during the Holocene (Figure 5e), which is also consistent with the dinocyst-based SST seasonal range.

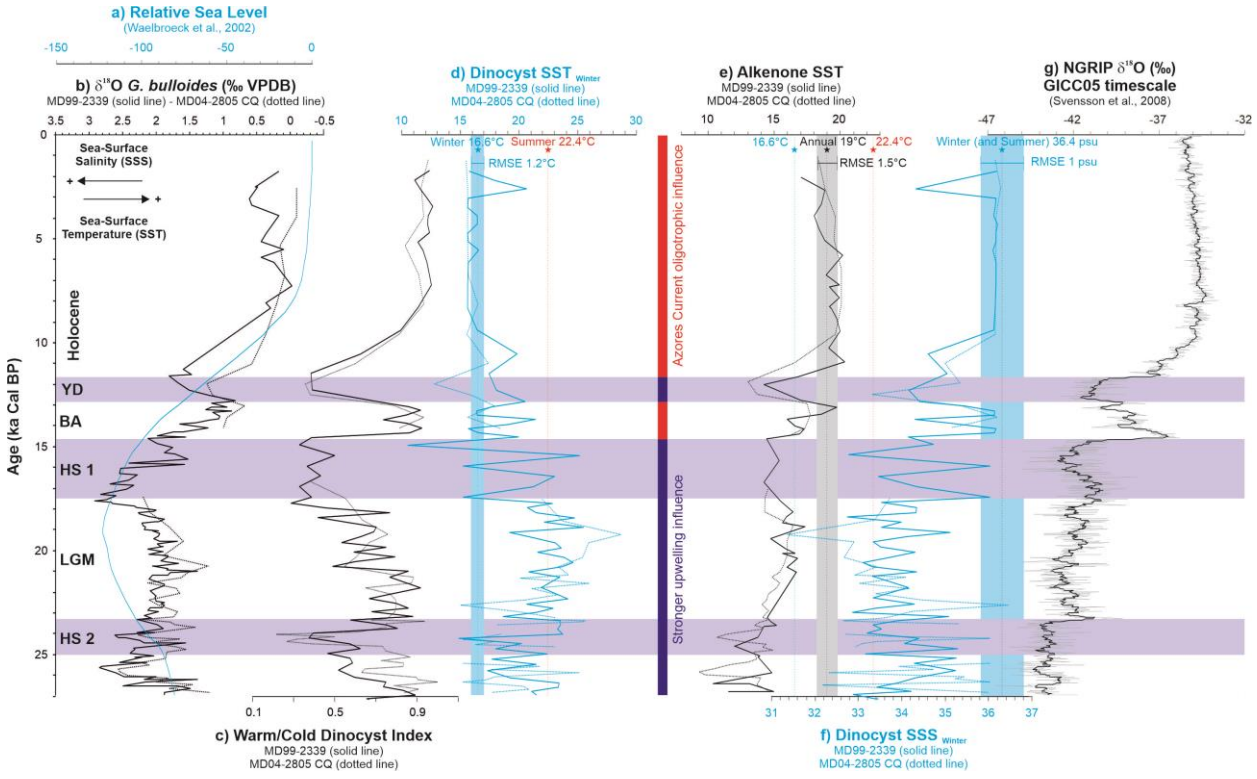

Figure 5: *Relative Sea Level (a) and glaciological $\delta^{18}O$ from NGRIP (g) in parallel with sea-surface hydrological quantifications performed on both study cores with dinocysts (d and f) and alkenones (e): MD99-2339 (central Cadiz) with solid lines and MD04-2805 CQ (southern Cadiz) with dotted lines. The dinocyst-derived qualitative paleothermometer index (Warm vs. Cold (Warm / Cold or W/C) dinocyst ratio is made according to Penaud et al., 2016 (c). W: Impagidinium taxa (I. aculeatum, I. paradoxum, I. sphaericum, I. strialatum, I. patulum) and Spiniferites taxa (S. delicatus, S. bentorii, S. mirabilis); and C: Bitectatodinium tepikiense, Spiniferites taxa (S. elongatus, S. lazus), Nematosphaeropsis labyrinthus, cysts of Pentapharsodinium dalei. SST: Sea Surface Temperature and SSS: Sea Surface Salinity. Modern values are highlighted with colored stars: present-day seasonal values for SST (16.6°C in Winter and 22.4°C in Summer) and SSS (36.4 psu for Winter and Summer seasons) estimates (cf. Figure 3 for mean values at both coring sites) have been averaged for an integrated view of the study investigated at a regional scale. Also, mean annual SSTs are of 18.5°C in central Cadiz and of 19.4°C in NW Morocco, providing the 19°C annual value highlighted in (e). Standard errors (RMSE) for each reconstructed parameter (d,e,f) are also represented and centered on seasonal (dinocyst-based SST or SSS) or annual (alkenone-based SST) present-day values. Data obtained on the 140-300 cm (cf. Figures 2 and 3) of core MD04-2805CQ are discarded from the discussion and are not represented in age. HS: Heinrich Stadial; LGM: Last Glacial Maximum; BA: Bölling-Alleröd; YD: Younger Dryas. Purple bands indicate HSs and the YD.*

4.1.2. The paradox raised by LGM reconstructions in the Gulf of Cadiz

Glacial dinocyst-based SST and SSS estimates (Figure 5c, d, and f) show high amplitude oscillations at the sub-millennial scale that are in line with the high climate variability recorded in the Northern Hemisphere during glacial times (Figure 5g). This is particularly evident for the millennial events of the Last Glacial Maximum (LGM; 23–19 ka BP), which have been documented in numerous regional sea-surface records such as those of the Celtic margin (Eynaud et al., 2012) and Nordic Seas (de Vernal et al., 2006; Caulle et al., 2013; Wary et al., 2017). Here, our reconstructions of LGM dinocyst-based SST indicate relatively warm summers (mean of 23.3°C for both study cores on the 23–19 ka BP interval: not shown here but available; cf. section 8) and winters (mean of 22.6°C for both study cores for the 23–19 ka BP interval) with some winter SST values as high or higher than present-day summer ones (mean of 22.4°C highlighted in Figure 5d,e averaging those of southern Cadiz, 22.7°C, and of central Cadiz, 22.1°C: cf. Figure 3). Even if there is growing evidence for warm LGM conditions, at least episodically, in the North Atlantic and European region from marine (e.g. Falardeau et al., 2018 and discussion therein) and terrestrial (e.g.

van der Bilt & Lane, 2019; Alsos et al., 2020) records, our dinocyst-based estimates appear striking and lead to caution about the absolute values of reconstructions in the study area. Here, the warm dinocyst-based SST estimates recorded during the LGM, regardless the season, might be biased towards high values, the best modern analogues being found in the Gulf of Guinea (Figures 3 and 4) due to the co-occurrence of *Brigantedinium* spp., *Lingulodinium machaerophorum* and *Operculodinium israelianum* taxa, the latter reaching up to 5% in both study cores only during the LGM (cf. Penaud et al., 2016). Among heterotrophic dinocyst taxa, the genus *Brigantedinium* is the most cosmopolitan one, occurring today at all latitudes, from nearshore to offshore settings (de Vernal et al., 2020). This cosmopolitan species has a widespread distribution from equatorial to polar Atlantic regions, including the western equatorial Atlantic and the coastal upwelling along the western African margin, within a broad range of temperatures and salinities (Marret and Zonneveld, 2003). This genus is often related with high primary productivity (e.g. Lewis et al., 1990; Dale and Fjellsafi, 1994; Marret, 1994; Biebow, 1996; Targarona et al., 1999; Zonneveld et al., 2001; Radi and de Vernal, 2004, 2008), including the study area (Marret, 1994; Penaud et al., 2010, 2011, 2016). In addition, since the highest proportions of *O. israelianum* are today recorded in surface sediments of the western African margin (5–10%; de Vernal et al., 2020), characterized by summer SST as high as 29°C and not below 24°C (Marret & Zonneveld, 2003), a bias towards abnormally high SSTs in the study area is possible. This illustrates perfectly the concept of analogues in statistics.

In contrast to dinocyst data, alkenone-based SST values point to cooler conditions (13.4°C on average; Figure 5e) than during the Holocene (19°C on average). As other proxies, alkenones have also limitations and they can yield biased temperature estimates in low salinity environments (e.g., Kucera et al., 2005; de Vernal et al., 2006; Marshall et al., 2021). It is worth noting that the long-term alkenone-based increasing SST trend from 27 ka BP onward (Figure 5e) follows a pattern similar to the long-term increasing trend of dinocyst-based SSS (Figure 5f), suggesting common forcing on these proxies including possibly a shift in seasonal hydrological conditions and/or upper water mass stratification. During the glacial period, an intensified and/or longer seasonal upwelling with haptophyte blooms, responsible for alkenones, may have resulted in a bias towards over-estimated cooler SSTs. A stronger upwelling activity and/or longer wind-driven upwelling season, as also testified by *Brigantedinium* spp., may then have accounted for cooler as well as less saline waters in the study area while, during the Holocene, warmer alkenone-based SSTs and higher dinocyst-based SSS may be due to the prevailing influence of the warmer and saltier Azores Current in a context of weaker upwelling and/or shorter seasonal upwelling intervals (Figure 5).

In addition, in the LGM section of both study cores, planktonic foraminifera are characterized by

relatively light $\delta^{18}O$ values (mean of 1.9 ‰ with peaks reaching 1.4 ‰; Figure 5b) compared to the entire glacial interval. Lower sea level during that period could have led to heavier values (Waelbroeck et al., 2002) and thus cannot explain the light $\delta^{18}O$ values. The light values indicate slightly lower SSS and/or slightly higher SST (Figure 5c and d). Although absolute dinocyst-based SST estimates must be interpreted with caution, the W/C index (Figure 5c), as alkenone-derived SST (Figure 5e), likely point out to generally slightly warmer SSTs during the LGM than during the two encompassing HS that experienced significant SST drops in the study area (e.g. Salgueiro et al., 2010, 2014; Patton et al., 2011; Penaud et al., 2011, 2016).

4.2. Productivity signals: from production to remineralization

4.2.1. General observations on past PP conditions

The climatic subdivisions identified in Figure 5 are also shown in Figure 6 to help us discuss PP conditions over the last 27 kyr BP. Dinocyst-based PP estimates (Figure 6b) follow previously reconstructed glacial-interglacial patterns in the intertropical Atlantic, with generally higher PP during the last glacial period than during the Holocene. Higher productivity during glacial times has been associated with increased wind-stress accompanied by i) enhanced aeolian dust availability of iron and micronutrients leading to fertilization of the surface ocean (Moreno et al., 2002; Bout-Roumazeilles et al., 2007; Wienberg et al., 2010), and ii) physical hydrographical processes leading to strong upwelling (Dupont et al., 1998; Shi et al., 1998; Dupont & Behling, 2006; Kim et al., 2010; Zonneveld et al., 2013; Penaud et al., 2016; Hardy et al., 2016, 2018). The long-term changes in productivity inferred by our dinocyst reconstructions (Figure 6b) lend further support to previous results from the same region based on a foraminiferal index (core GeoB 9064 from the central GoC; Wienberg et al., 2010; Figure 6c).

4.2.2. Remineralization processes

In core MD04-2805 CQ, the benthic $\Delta\delta^{13}C$ offset (Figure 6e) provides information on the respired carbon at the core site (859 m deep off NW Morocco), with high $\Delta\delta^{13}C$ values indicating high remineralization release of isotopically light $\delta^{13}C$ to pore waters (McCorkle & Emerson, 1988; Gehlen et al., 1999). This approach has been used in cores encompassing the LGM and Holocene in the Eastern Equatorial Pacific Ocean (Umling & Thunell, 2018, with shallow infaunal foraminifera) and sub-Antarctic Atlantic Ocean (Gottschalk et al., 2016a, with deep infaunal foraminifera) to provide information on organic matter flux to the seafloor and, thus, information on the export

productivity. Close to our study area, on the Iberian margin at 3,146 m water depth, $\Delta\delta^{13}C$ between epifaunal *Cibicidoides* and deep infaunal *Globobulimina* was further used by Hoogakker et al. (2015) to reconstruct bottom-water oxygen concentrations over the past 150 kyr. In our study area, higher $\Delta\delta^{13}C$ values (Figure 6e) are generally observed during the glacial interval (mean of 1.1 ‰, standard deviation of 0.4 ‰), while lower $\Delta\delta^{13}C$ values characterize the Holocene (mean 0.7‰, standard deviation of 0.2‰), suggesting generally higher rates of organic carbon respiration during high glacial PP periods (Figures 6b and c). In contrast, the Holocene is characterized by low dinocyst fluxes and the establishment of oligotrophic conditions (Penaud et al., 2016), thus implying reduced export production, and reduced organic matter respiration or remineralization (Figure 6e).

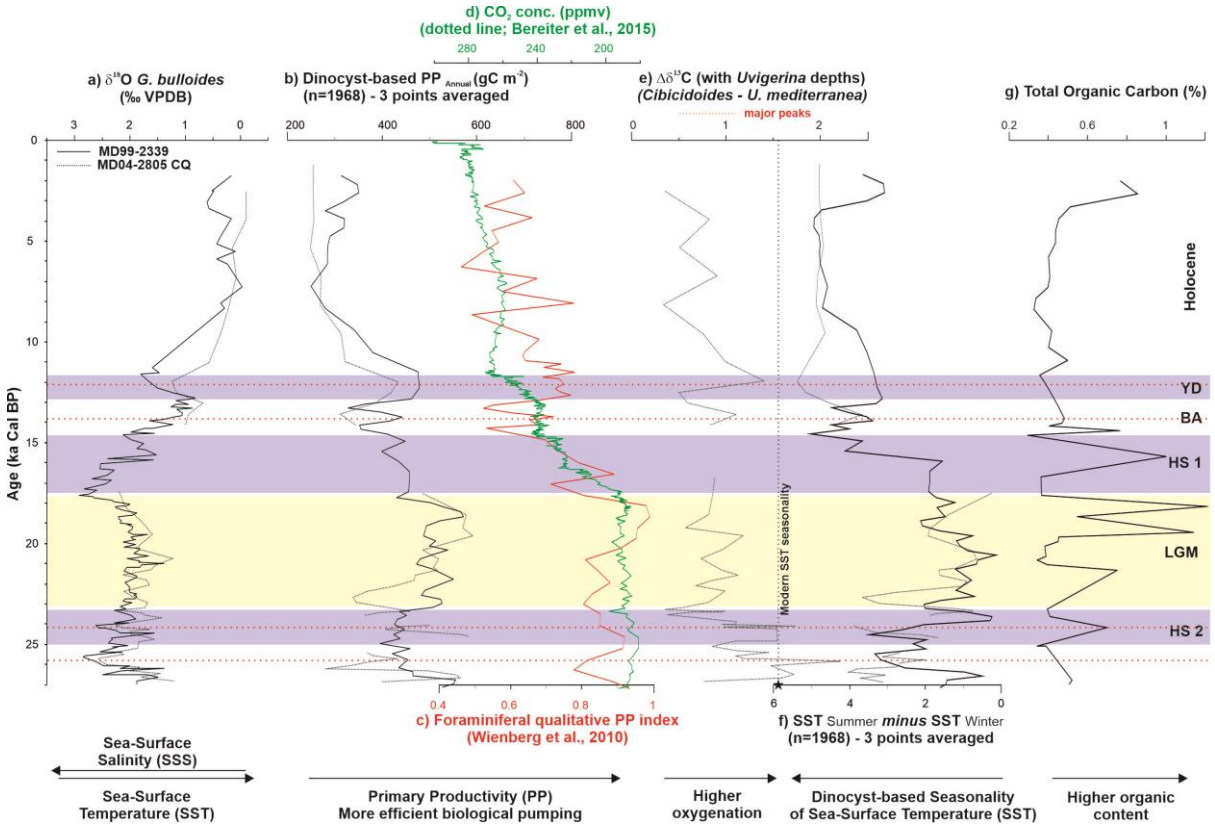

Figure 6: *$CO_{2\ atm}$ concentrations (d) and foraminiferal-based Primary Productivity (PP) qualitative information (c) in parallel with selected proxies acquired on both study cores (dotted lines for core MD04-2805 CQ, southern Cadiz, and solid lines for core MD99-2339, central Cadiz): planktonic $\delta^{18}O$ data (a), dinocyst-based PP (b) and SST seasonality (f) were acquired for both cores, benthic $\Delta\delta^{13}C$ (e) is only available for the southern Cadiz core and the Total Organic Carbon (g) is only available for the central Cadiz core. Red horizontal dotted lines highlight the major peaks recorded*

with the $\Delta\delta^{13}C$ proxy. Data obtained on the 140-300 cm (cf. Figures 2 and 3) of core MD04-2805CQ are discarded from the discussion and are not represented in age. HS: Heinrich Stadial; LGM: Last Glacial Maximum; BA: Bölling-Alleröd; YD: Younger Dryas. Purple bands indicate HSs and the YD.

4.3. Hypothesized links between PP and seasonality

Canonical Correspondence Analysis (CCA; Figure 7) was applied to dinocyst assemblages of core MD04-2805 CQ. A group of thermophilic taxa characteristic of full-oceanic oligotrophic conditions (*Spiniferites mirabilis* and *Impagidinium* spp.) appears distinct from taxa with an affinity for cold environments (*Bitectatodinium tepikiense*, *Spiniferites elongatus* and *Spiniferites lazus*) (Figure 7). Heterotrophic taxa that are generally associated with strong upwelling in modern environments (Marret & Zonneveld, 2003; Radi & de Vernal, 2008) are closer to the cold group of taxa. In contrast, *Lingulodinium machaerophorum*, which is often related to water mass stratification, is closer to the group of warm taxa; the latter group being mainly related to high annual and summer SST (as shown by alkenone- and dinocyst-based estimates, respectively) as well as to high SSS (Azores Current influence). This distribution is consistent with cold and nutrient-rich waters in the glacial period and more specifically during stadials (Penaud et al., 2010, 2011, 2016), in contrast to warm and thermally stratified oligotrophic waters such as found today. In addition, high dinocyst-based PP estimates are distributed along the same axis as high planktonic $\delta^{18}O$, hence supporting the argument of enhanced PP in the studied area during the glacial period. We also included the benthic $\Delta\delta^{13}C$ signal as an environmental variable in the CCA (Figure 7). It shows an inverse relationship with the planktonic $\delta^{13}C$ signal (Figure 7), further supporting the hypothesis of an opposition between low productivity (Penaud et al., 2010; Frihmat et al., 2015) and high remineralization under oxic conditions (Hoogaker et al., 2015). We also included SST and SSS seasonality variables in the CCA (Figure 7), knowing that today's seasonal-scale processes impact the hydrographical conditions in the GoC (Garcia Lafuente & Ruiz, 2007). Seasonal contrasts of SST and SSS might thus have influenced the plankton dynamics during the last glacial cycle offshore of Portugal (Datema et al., 2019). Therefore, we suggest two potential links as follows (Figure 7): i) high organic matter remineralization and high SST seasonal contrast (likely related to colder winter seasons), and ii) high PP conditions and high SSS seasonal contrast (likely related to seasonal salinity drops).

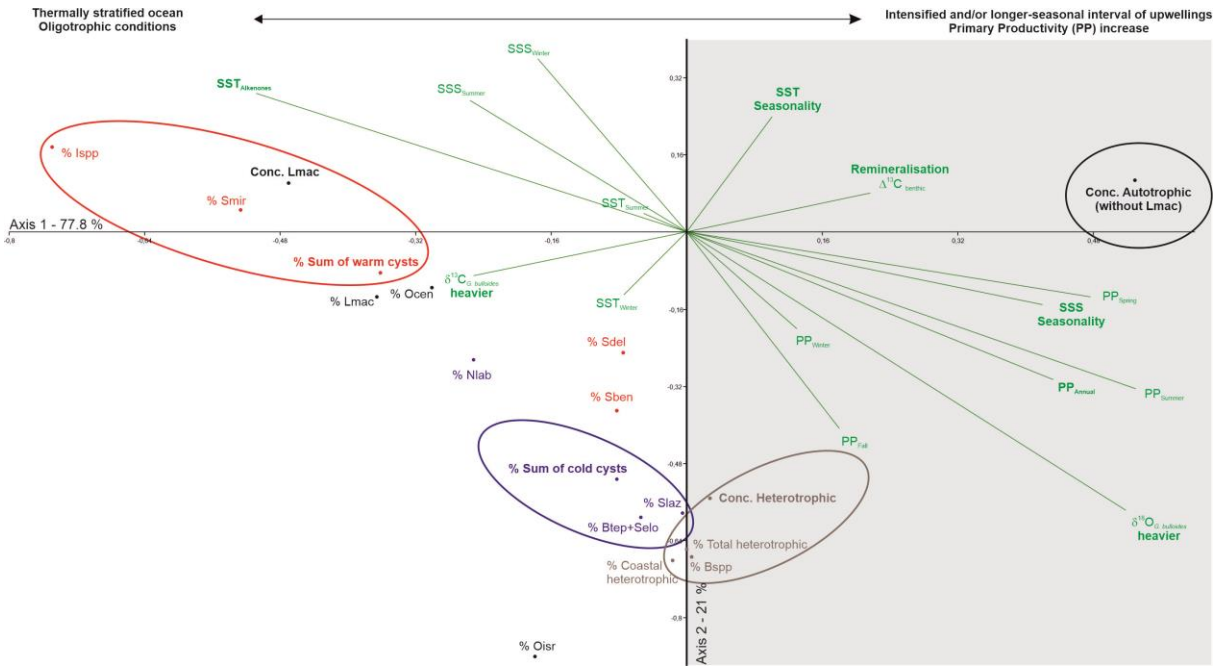

Figure 7: *Canonical Correspondence Analysis (CCA) performed with the Past version 1.75b software (Hammer et al., 2001) to dinocyst assemblages (expressed in percentages "%" and absolute concentrations "conc.") of core MD04-2805 CQ (cf. Penaud et al., 2010, 2011 for a complete visualization of dinocyst results) to capture the main factors (i.e. environmental variables including stable isotope data, alkenone-based SST and dinocyst-based quantifications) that could typify the productivity control in the study area. SST: Sea Surface Temperature; SSS: Sea Surface Salinity; PP: Primary Productivity. Ispp: Impagidinium species; Lmac: Lingulodinium machaerophorum; Ocen: Operculodinium centrocarpum; Oisr: Operculodinium israelianum; Nlab: Nematosphaeropsis labyrinthus; Btep: Bitectatodinium tepikiense; Bspp: Brigantedinium species; Spiniferites species: S. mirabilis (Smir), S. delicatus (Sdel), S. bentorii (Sben), S. lazus (Slaz), S. elongatus (Selo). Red and blue colors for dinocyst taxa codes refer, respectively, to Warm (W) and Cold (C) taxa identified in the W/C index (Figure 5c). Brown color for dinocyst taxa codes refer to heterotrophic taxa.*

5. MD04-2805 CQ and MD99-2339 cores: a new look at the carbon cycle along an Eastern Boundary Current over the last 50 kyr

Present-day processes on the northern GoC platform (Garcia Lafuente et al., 2006; Garcia Lafuente & Ruiz, 2007) are driven by westerlies inducing upwelling off southern Iberia (northwestern GoC), with filaments directed southward to the open GoC (i.e. stronger cyclonic eddy off cape San Vincente in Figure 8). This mechanism diverts waters from the northwestern shelf to the open GoC. On the contrary, under easterlies, a westward coastal counter-current (i.e. CCC in Figure 8) allows the connection of the highly productive and wider northeastern GoC shelf, influenced by strong fluvial discharges, to the northwestern GoC shelf (Garcia Lafuente et al., 2006; Garcia Lafuente & Ruiz, 2007). We thus expect to record higher numbers of heterotrophic species in the GoC under strong-dominant westerlies, and higher fluvial-sensitive taxa such as *L. machaerophorum* under strong-dominant easterlies. Also, under modern conditions, continental shelf dynamics and PP show a clear seasonal and inter-annual signal in the northern GoC (Garcia Lafuente & Ruiz, 2007). Here, we combine this knowledge of modern oceanography and seasonality with that of past productivity, seasonality, and remineralization to address the long-term carbon cycle in the GoC, which could be used as a regional model for understanding an EBC system of the North Atlantic subtropical gyre.

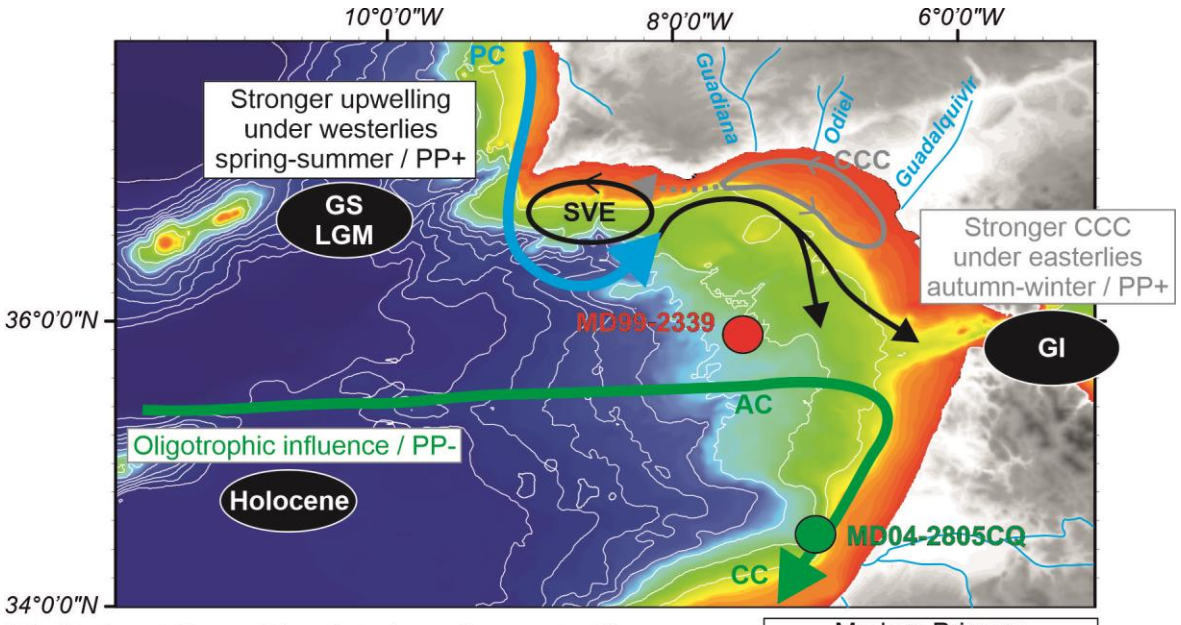

Figure 8: *Sketch of the circulation in the Gulf of Cadiz according to the model of Garcia Lafuente et al. (2006). Study cores MD04-2805 CQ and MD99-2339 are indicated on the map, also depicting the bathymetry of the study area (cf. Figure 1). The Portugal Current (PC) flows southward from 45°N to 30°N. The Azores Current (AC), derived from the southern branch of the Gulf Stream, flows eastward to the Gulf of Cadiz at about 35°N. The Canary Current (CC) is fed by both the AC and the PC. The seasonal strengthening of western and eastern cyclonic eddies on the northern Gulf of Cadiz shelf are highlighted in the Figure according to the present-day understanding of hydrological processes. Prevailing "spring-summer" pattern is highlighted for Greenland Stadials (GS) and the Last Glacial Maximum (LGM) while strengthening of the "autumn-winter" pattern (synchronization of the higher rainfall pattern with the CCC) is highlighted for Greenland Interstadials (GI). Today, and during the Holocene in general, the Gulf of Cadiz is mainly characterized by an oligotrophic regime associated with nutrient-poor waters carried by the AC.*

5.1. Paleoproductivity changes over the last 50 kyr in the Gulf of Cadiz

Our new PP estimates (Figure 9b) are in line with the observed decrease in dinocyst fluxes from the glacial to the Holocene (Penaud et al., 2016), and provide evidence for a three-step decrease: i) the 27–50 ka BP interval with PP_{annual} peaks higher than 600 gC m^{-2} ("A" window, Figure 9); ii) the 11–27 ka BP interval with high PP_{annual} of 430–600 gC m^{-2} ("B" window, Figure 9); and iii) the 0–11 ka BP interval characterized by the lowest PP_{annual} values, as low as 250 gC m^{-2} ("C" window, Figure 9). This three-step scheme is discussed below.

5.1.1. The 27–50 ka BP interval

Strong PP peaks occurred during MIS 3 (Figure 9b), especially during Greenland Interstadials (GIs; Figure 9a). In the GoC, present-day nutrient concentrations are generally low but relatively high at the mouth of the Guadalquivir River (cf. Figure 8), which is also the most productive area of the GoC (i.e. the GoC is oligotrophic elsewhere, Navarro & Ruiz, 2006; Garcia Lafuente & Ruiz, 2007). High MIS 3 PP peaks, coinciding with low values of the "Distance to the Coast" (DC) index (Figure 9f), may be related to nutrient replenishments of surface waters by intensified runoff carrying dissolved or suspended substances from the continent under warm and humid climate GI conditions. Indeed, beyond the changes related to the global mean sea level (Figure 9g; Waelbroeck et al., 2002), the particularly low DC excursions (Figure 9f), which are linked to coastal dinocyst taxa, suggest strong riverine inputs during PP increases (Figure 9b). We, therefore, suggest that the rainfall pattern led to enhanced frequencies of flooding events on the northern shelf of the GoC

margin and possibly more largely in eastern subtropical Atlantic latitudes, as reconstructed for the hinterland of the Cariaco Basin in the western subtropical North Atlantic (González et al., 2008; Deplazes et al., 2019). In order to explain observations from the study site (MD99-2339, central GoC), we propose an efficient warm counter-current in the northern GoC (cf. Figure 8) as observed today during phases of intense easterlies (present-day meteorological model of García Lafuente et al., 2006; Garcia Lafuente & Ruiz, 2007). Interestingly, between 32 and 27 ka BP, high PP peaks (Figure 9b) and low DC indices (Figure 9f) correspond to low *L. machaerophorum* percentages (Figure 9c), while high PP peaks and low DC indices correspond to extremely high *L. machaerophorum* percentages during GIs 12 and 8, even reaching percentages as high as those found in present-day western French estuaries (Morzadec-Kerfourn, 1977; Ganne et al., 2016; Penaud et al., 2020). We suggest that *L. machaerophorum* occurrences during GIs 12 and 8 reflect interstadial conditions long enough to sustain stabilization of fluvial systems, and the development and fixation of riparian vegetation on riverbanks (Penaud et al., 2020), such as during the Bölling-Alleröd and the Holocene. Enhanced fluvial input may then explain the co-occurrence of high SST, low SSS and high PP during GI, in opposition to low SST and low SSS due to upwelling-induced PP increases reconstructed during GS.

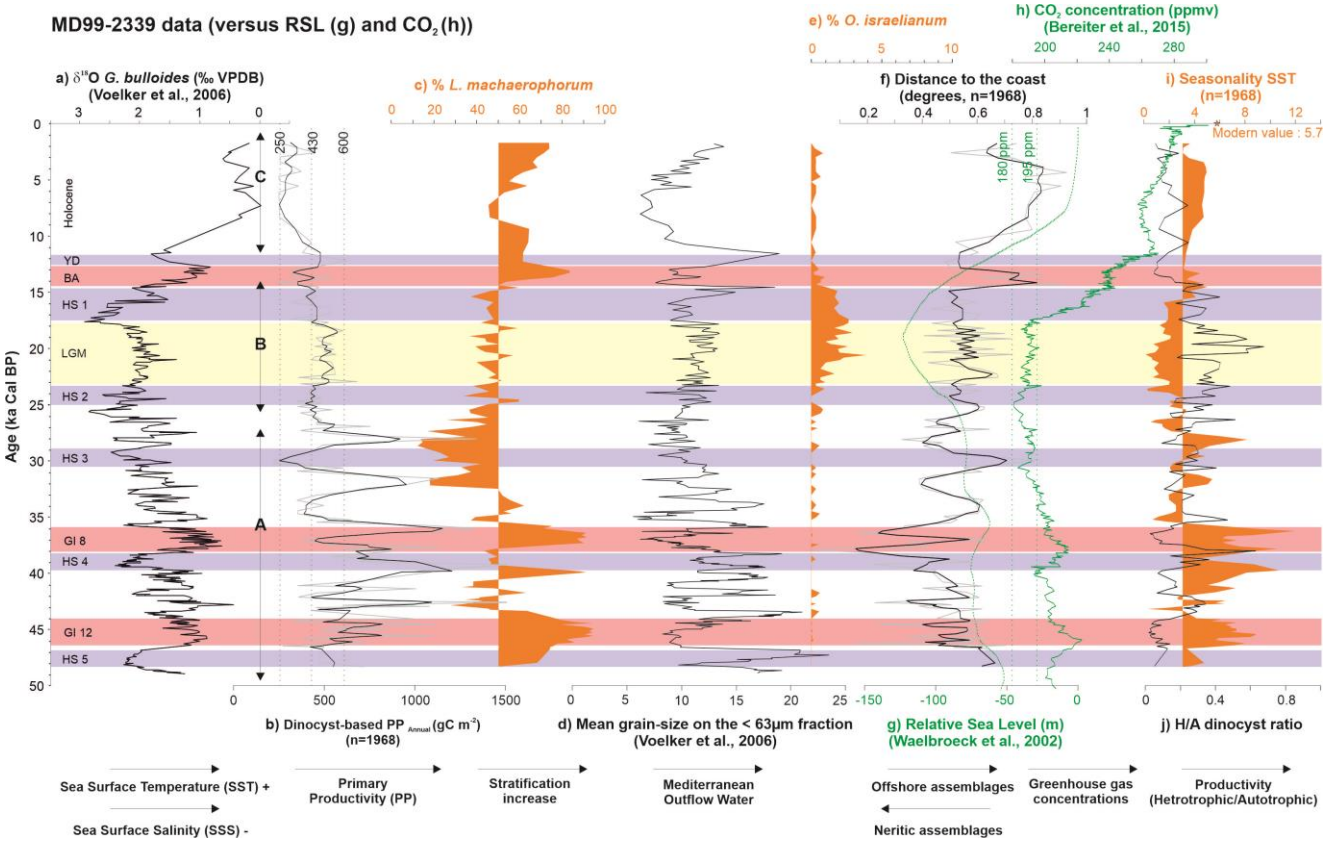

Figure 9: *Relative sea level curve (g) and $CO_{2\ atm}$ concentrations (h) in parallel with selected proxies acquired on core MD99-2339: planktonic $\delta^{18}O$ (a) and mean-grain size of the fine fraction (d), dinocyst percentages (c,e), Heterotrophic vs. Autotrophic (H/A) dinocyst ratio (j; cf. Penaud et al., 2016), and dinocyst-based parameters (b: Primary Productivity or PP, f: Distance to the coast index, and i: Sea Surface Temperature or SST seasonality). HS: Heinrich Stadial; GI: Greenland Interstadial; LGM: Last Glacial Maximum; BA: Bölling-Alleröd; YD: Younger Dryas. Purple bands indicate HSs and the YD, pink bands indicate GIs 8 and 12 and the BA.*

5.1.2. The 11–27 ka BP interval

The 11–27 ka interval encompasses HS1, HS2, and the LGM. In the study area, this interval may be characterized by an intensified and/or longer seasonal interval of spring–summer upwelling, as indicated by the high Heterotrophic vs. Autotrophic (H/A) ratio (cf. Penaud et al., 2016; Figure 9j; Datema et al., 2019), which promoted higher PP than today (Figure 9b). Today, strengthened upwelling are suggested to occur under strong westerlies (cf. Figure 8), according to the present-day meteorological model of Garcia Lafuente & Ruiz (2007). In addition to spring–summer upwelling that may account for cooler glacial alkenone-derived SST than dinocyst-derived ones (Figure 5e), the occurrence of the species *O. israelianum* (Figure 9e), today characterized by temperate–tropical distributions in surface sediments from the Northern Hemisphere database (e.g., de Vernal and Marret, 2007; Marret et al., 2008; Zonneveld et al., 2013; Limoges et al., 2013; de Vernal et al., 2020), may suggest higher SSTs in winter, thus accounting for the low seasonal contrast in SST estimates (Figure 9i), with cooler summers (at times of upwelled waters) and warmer winters (at times of upwelling relaxation).

5.1.3. The 0-11 ka BP interval

In our study, the Holocene interval ("C" window, Figure 9) seems to be characterized by a relatively strong SST seasonality (Figure 9i), which is similar to modern conditions (around 6°C). Oligotrophic waters (low PP, Figure 9b) are thermally stratified, as suggested by the high percentages of *L. machaerophorum* (Figure 9c) – a taxon typical of estuarine environments (Morzadec-Kerfourn, 1977; Ganne et al., 2016; Penaud et al., 2020). The GoC is today under the oligotrophic influence of the Azores Current (cf. Figure 8) and is characterized by a marked seasonal gradient of temperature that exerts a strong control on chlorophyll concentrations (Garcia Lafuente & Ruiz, 2007; Prieto et al., 2009), combined with the seasonal influence of river discharges in autumn–winter (i.e. at times of higher rainfall; see introduction to section 2.; cf. Figure 8). Our Holocene reconstructions, therefore, fit these modern observations.

5.2. Implications of PP regimes in EBC systems for $CO_{2\ atm}$ changes

5.2.1. Importance of biogeochemical cycles in $CO_{2\ atm}$ variations

It was hypothesized that enhanced PP contributed significantly to the $CO_{2\ atm}$ drawdown during glacial times (e.g. Broecker, 1982). Indeed, biogeochemical mechanisms need to be taken into account (e.g. Buchanan et al., 2016; Galbraith & Jaccard, 2015; Schmittner & Somes, 2016) with physical processes (inducing gas solubility or atmosphere-ocean exchange of CO_2 and ocean circulation; e.g. Hain et al., 2010; Gottschalk et al., 2016b) to understand the carbon cycle. Many studies have suggested that, during glacial intervals, circulation in the Southern Ocean acted as a driver of $CO_{2\ atm}$ changes through strengthened AABW formation and/or enhanced nutrient uptake (e.g. Sarmiento & Toggweiler, 1984; Marinov et al., 2006; Gottschalk et al., 2016b; Jansen, 2017). In addition, studies also revealed the impact of increased sediment exposure and subsequent silicate weathering during low sea level stands for explaining the $CO_{2\ atm}$ drawdown (Wan et al., 2017). Hence, as highlighted by Gottschalk et al. (2019), high temporal resolution reconstructions at the regional scale, such as this study, are necessary to quantify environmental changes accompanying $CO_{2\ atm}$ variations, especially for constraining some parameters in modeling studies.

Today, the GoC is characterized by an oligotrophic regime (nutrient-poor waters carried by the Azores Current) and is associated with low CO_2 storage (Huertas et al., 2006, 2009; Flecha et al., 2012), as previously discussed with respect to the Holocene. However, the last 50 kyr have been characterized by different glacial PP regimes, which thus influenced carbon export to the seafloor, along with variable conditions of carbon sequestration *versus* remineralization through time that likely had consequences for the carbon cycle. Dinocyst-based (Figure 6b) and foraminiferal-based (Figure 6c) PP reconstructions, obtained independently on different cores, point to changes consistent with the $CO_{2\ atm}$ drawdown (Bereiter et al., 2015; Figure 6d) by recording similar timing and rate of change. We may thus consider how our study site evolved regarding carbon remineralization *versus* sequestration as a model for an Eastern Boundary Current (EBC) under a glacial climate.

5.2.2. Carbon sequestration across the LGM

At glacial–interglacial (orbital) timescales, we have discussed the link between PP and $\Delta\delta^{13}C$ (see subsection 4.2.), which generally fluctuate together, with stronger remineralization during higher PP and *vice versa* (southern Cadiz; Figure 6). A more complex scheme is depicted at the millennial timescale in the reconstructions of core MD04-2805 CQ. Indeed, a positive relationship between PP (Figure 6b,c) and $\Delta\delta^{13}C$ (Figure 6e) still characterizes the last 15 kyr (dotted lines at ca. 12 and 14

ka BP; Figure 6) and, before 18 ka, high PP reconstructed during the LGM does not coincide with significant increases in $\Delta\delta^{13}C$ (Figure 6e) while significant peaks in TOC values (reaching 1%) are occasionally found in core MD99-2339 (Figure 6g). Therefore, sustained LGM-PP (Figure 6b) combined with moderate remineralization rates may have offered favorable conditions for carbon sequestration, at least between 859 m and 1,170 m depth over the studied area. It is worth noting that low organic matter remineralization when PP remains high may be explained by reduced bottom-water oxygen concentrations. This would also be consistent, during the LGM, with: i) poor ventilation promoting the accumulation of a respired carbon pool at 1–3 km depth (e.g. Buchanan et al., 2016; Umling & Thunell, 2017, 2018); ii) reduced bottom-water dissolved oxygen concentrations along the southern Iberian margin (Hoogakker et al., 2015); and iii) reduced and weakly oscillating Mediterranean Outflow Water intensity (MOW; Voelker et al., 2006; Figure 9d) at our study site, keeping in mind that the GoC study area lies beyond the reach of the MOW as it did during the glacial period (e.g. Eberwein & Mackensen, 2008; Rogerson et al., 2011). Because the lowest $CO_{2\ atm}$ concentrations were reached at around 25 ka BP (Figure 9i), we hypothesize that the increase in respired carbon storage at mid-depths (850–1200 m water depth) could have contributed to maintaining low atmospheric CO_2 concentrations during the LGM through an efficient biological pump. The mechanism we propose here is based on a regional dataset but could be applied at a larger scale to explain, at least partly, atmospheric CO_2 changes through time.

5.2.3. Carbon sequestration across GIs 12 and 8

Pronounced MOW millennial-scale variability was recorded during MIS 3 (Voelker et al., 2006; Figure 9d), which likely implies variable oxygenation in bottom waters at the study site. We may expect that lower remineralization followed the slowdown of the MOW during the interstadials, as discussed for the LGM, and conversely during the stadials. During GIs 12 and 8, the highest *L. machaerophorum* percentages coincide with two major atmospheric $CO_{2\ atm}$ declines shaping the long-term trend across the glacial period (Figure 9i). We suggest that prolonged intervals of organic matter deposition from both terrestrial and marine sources into a poorly oxygenated basin may have contributed to increasing carbon sequestration in the GoC. The magnitude of $CO_{2\ atm}$ rise has been shown to be largely determined by the stadial duration (Gottschalk et al., 2020). Here, we suggest that the corollary may be true for the long interstadials as being favorable to an ocean sink of $CO_{2\ atm}$.

6. Conclusion

This study addresses the oceanographic response of the GoC to complex continent–ocean interactions. Today, this region is characterized by low to moderate PP, the oligotrophic regime being related to nutrient-poor water advection from the Azores Current. In contrast, the area was characterized by high PP during the last glacial period. In this study, the multi-proxy dataset includes new stable isotope data of epibenthic foraminifera *C. pachyderma–C. wuellerstorfi*, allowing estimation of organic matter export and remineralization processes through the benthic epifaunal-infaunal $\delta^{13}C$ gradient ($\Delta\delta^{13}C$), in addition to new dinocyst-based PP estimates reconstructed with the new enlarged n = 1,968 dinocyst database. Our results show high PP during the glacial period and the establishment of oligotrophic conditions from the onset of the Holocene. High benthic $\Delta\delta^{13}C$ excursions and high PP were generally observed for the glacial period, in contrast to the Holocene, also suggesting higher carbon export and remineralization. We furthermore show, based on dinocyst-based estimates, that seasonal gradients in SST and SSS were potential drivers of productivity changes over the last 50 kyr. During MIS 3, particularly high PP may be related to nutrient replenishments in surface waters by runoff, as shown by neritic dinocyst assemblages and peak nutrient concentrations during the warmer and humid climate phases of Greenland interstadials, also characterized by strong seasonal contrasts in both SSS and SST. During MIS 2, and more specifically across the LGM, extremely low dinocyst-based SST seasonality due to warmer winters and colder summer conditions were reconstructed. We suggest that intensified and/or longer seasonal functioning of upwelling allowed the maintenance of sustained PP levels, although lower than during MIS 3, combined with lower remineralization of organic matter contributing to carbon sequestration at that time. Finally, the Holocene is characterized by the establishment of oligotrophic conditions with reduced organic matter export in parallel with reduced oxic respiration. The Gulf of Cadiz is not presently a carbon sink; however, this study demonstrates that its state was different under glacial regimes. Hence, our study may help to improve understanding of variations in the carbon cycle along Eastern Boundary Currents (EBC) under glacial and interglacial climates, thus providing new elements to consider in global biogeochemical models.

7. Acknowledgements

Thanks are due to the French polar institute (IPEV, *Institut Paul Emile Victor*), the captain and the crew of the Marion Dufresne, and the scientific teams of the IMAGES I and V cruises. Part of the analyses of this study was supported by the French CNRS and contributes to the 2013 INSU project

“ICE-BIO-RAM: *Impact des Changements Environnementaux sur la BIOdiversité marine lors des Réchauffements Abrupts du climate*”. CW and FE acknowledge support from the European Research Council grant ACCLIMATE/n° 339108. This study was also partly supported by the National Research Foundation of Korea (NRF) grant funded through the Ministry of Science and ICT (NRF-2021M1A5A1075512). We acknowledge the French Ministry for Europe and Foreign Affairs (MEAE), the Ministry of Higher Education, Research and Innovation (MESRI), the National Research Foundation of Korea (NRF) as well as the Korean Ministry of Science and ICT (MSIT) through its international Hubert Curien (PHC) partnership programme STAR between France and Republic of Korea to financially support the MEDKO (Abrupt Climate events in the past Mediterranean and Korean basins) project that financially supported the alkenone-based SST record of core MD99-2339. We are also grateful to Prof. Shin for his considerable analytical support and access to lab facilities at Hanyang University, Republic of Korea. DO acknowledges funding from Portuguese Foundation for Science and Technology (FCT) through the CCMAR FCT Research Unit - project UIDB/04326/2020 and contract (CEECIND/02208/2017). Finally, we would like to thank the *Bureau de traduction* of the University of Brest for the improvement of English, and the two reviewers, including André Bahr, for their constructive and precise comments.

8. Data availability

Data (Figure S1, as well as Tables S1 and S2 including age constraints of cores MD04-2805Q and MD99-2339 as well as all data acquired on both cores and discussed in the manuscript) are available in the Zenodo repository: https://doi.org/10.5281/zenodo.5573079.

9. References

Aristegui, J., Alvarez-Salgado, X.A., Barton, E.D., Figueiras, F.G., Hernandez-Leon, S., Roy, C., Santos, A.M.P., 2005. Chapter 23: oceanography and fisheries of the Canary current/Iberian region of the eastern North Atlantic (18a, E). In: Brink K.H. (ed.), Robinson A.R. (ed.) The sea: the global coastal ocean: interdisciplinary regional studies and syntheses. Harvard: Harvard University Press, 877–931.

Alsos, I.G., Sjögren, P., Brown, A.G., Gielly, L., Merkel, M.K.F., Paus, A., Lammers, Y., Edwards, M.E., Alm, T., Leng, M., Goslar, T., Langdon, C.T., Bakke, J., van der Bilt, W.G.M., 2020. Last Glacial Maximum environmental conditions at Andøya, northern Norway; evidence for a northern ice-edge ecological "hotspot". Quaternary Science Reviews 239, 106364.

Bereiter, B. et al. Revision of the EPICA Dome C CO2 record from 800 to 600 kyr before present. Geophysical Research Letters 42, 542–549.

Biebow, N., 1996. Geomar Report, 57: Dino£agellatenzysten als indikatoren der spa«t- und postglazialen entwicklung des auftriebgeshehens vor Peru. Geomar, Kiel, 130 pp.

Broecker, W.S., 1982. Ocean chemistry during glacial time. Geochimica et Cosmochimica Acta 46 (10), 1689–1705.

Bout-Roumazeilles, V., Combourieu Nebout, N., Peyron, O., Cortijo, E., Landais, A., Masson-Delmotte, V., 2007. Connection between South Mediterranean climate and North African atmospheric circulation during the last 50 000 yr BP North Atlantic cold events, Quaternary Sci. Rev., 26, 3197–3215.

Buchanan, P.J., Matear, R.J., Lenton, A., Phipps, S.J., Chase, Z., Etheridge, D.M., 2016. The simulated climate of the Last Glacial Maximum and insights into the global marine carbon cycle. Clim. Past 12 (12), 2271–2295.

Caballero, I., Morris, E.P., Prieto, L., Navarro, G., 2014. The influence of the Guadalquivir River on the spatio-temporal variability of suspended solids and chlorophyll in the Eastern Gulf of Cadiz. Medit. Mar. Sci. 15 (4), 721–738.

Coplen, T.B., 1988. Normalization of oxygen and hydrogen isotope data. Chem. Geol. 72, 293–297.

Caulle C., Penaud A., Eynaud F., Zaragosi S., Roche D., Michel E., Boulay S., Richter T., 2013. Sea-surface hydrographical conditions off South Faeroes and within the North-Eastern North Atlantic through MIS 2: the response of dinocysts. Journal of Quaternary Science 28, 217–228.

Dale, B., Fjellsa, A., 1994. Dino£agellate cysts as paleoproductivity indicators: state of the art, potential, and limits. In: Zahn, R., Pedersen, T.F., Kaminski, M.A., Labeyrie, L. (Eds.), NATO ASI Series I : Global Environmental Change, 17: Carbon Cycling in the Glacial Ocean: Constraints on the Ocean's Role in Global Change. Springer, Berlin, pp. 521–537.

Datema, M., Sangiorgi, F., de Vernal, A., Reichart, G.J., Lourens, L.J., Sluijs, A., 2019. Millennial-Scale Climate Variability and Dinoflagellate-Cyst-Based Seasonality Changes Over the Last ~150 kyrs at "Shackleton Site" U1385. Paleoceanography and Paleoclimatology, 34, 1139–1156.

de Haas, H., Mienis, F., Frank, N., Richter, T.O., Steinbacher, R., de Stigter, H., van der Land, C., van Weering, T.C.E., 2009. Morphology and sedimentology of (clustered) cold-water coral mounds at the south Rockall Trough margins, NE Atlantic Ocean. Facies 55, 1–26.

de Vernal, A., Marret, F., 2007. Organic-walled dinoflagellates : tracers of sea-surface conditions. In: Hillaire-Marcel, C., de Vernal, A. (Eds.), Proxies in Late Cenozoic Paleoceanography. Elsevier, pp. 371–408.

de Vernal, A., Eynaud, F., Henry, M., Hillaire-Marcel, C., Londeix, L., Mangin, S., Matthiessen, J., Marret, F., Radi, T., Rochon, A., Solignac, S., Turon, J.L., 2005. Reconstruction of sea-surface conditions at middle to high latitudes of the Northern Hemisphere during the last glacial maximum (LGM) based on dinoflagellate cyst assemblages. Quat. Sci. Rev. 24, 897–924.

de Vernal, A., Rosell-Mele c, A., Kucera, M., Hillaire-Marcel, C., Eynaud, F., Weinelt, M., Dokken, T., Kageyama, M., 2006. Comparing proxies for the reconstruction of LGM sea-surface conditions in the northern North Atlantic. Quaternary Science Reviews 25 (21–22), 2820–2834.

de Vernal, A., Rochon, A., Fréchette, B., Henry, M., Radi, T., Solignac, S., 2013. Reconstructing past sea ice cover of the Northern Hemisphere from dinocyst assemblages: Status of the approach. Quaternary Science Reviews 79, 122–134.

de Vernal, A., Radi, T., Zaragosi, S., Van Nieuwenhove, N., Rochon, A., Allan, E., De Schepper, S., Eynaud, F., Head, M., Limoges, A., Londeix, L., Marret, F., Matthiessen, J., Penaud, A., Pospelova, V., Price, A., Richerol, T., 2020. Distribution of common modern dinocyst taxa in surface sediments of the Northern Hemisphere in relation to environmental parameters: the updated n=1968 database. Marine Micropaleontology 159, 101796.

Deplazes, G., Nele Meckler, A., Peterson, L.C., Hamann, Y., Aeschlimann, B., Günther, D., Martínez-García, A., Haug, G.H., 2019. Fingerprint of tropical climate variability and sea level in sediments of the Cariaco Basin during the last glacial period. Sedimentology 66 (5), 1967–1988.

Dorschel, B., Hebbeln, D., Rüggeberg, A., Dullo, W.-C., 2005. Growth and erosion of a cold-water coral covered carbonate mound in the Northeast Atlantic during the Late Pleistocene and Holocene. Earth Planet. Sci. Lett. 233, 33–44.

Duplessy, J.C., Shackleton, N.J., Matthews, R.K., Prell, W.L., Ruddiman, W.F., Caralp, M.C., Hendy, C.H., 1984. 13C record of benthic foraminifera in the Last Interglacial Ocean: implications for the carbon cycle and the global deep water circulation. Quaternary Research 21, 225–243.

Duplessy, J.C., Shackleton, N.J., Fairbanks, R.G., Labeyrie, L., Oppo, D.W., Kallel, N., 1988. Deepwater source variations during the last climatic cycle and their impact on the global deepwater circulation. Paleoceanography 3 (3), 343–360.

Dupont, L., Behling, H., 2006. Land–sea linkages during deglaciation: High-resolution records from the eastern Atlantic off the coast of Namibia and Angola (ODP site 1078). Quatern. Int. 148, 19–28.

Dupont, L., Marret, F., Winn, K., 1998. Land-sea correlation by means of terrestrial and marine palynomorphs from the equatorial East Atlantic: phasing of SE trade winds and the oceanic productivity. Palaeogeography, Palaeoclimatology, Palaeoecology 142, 51–84.

Eberwein, A., Mackensen, A., 2006. Regional primary productivity differences off Morocco (NW-Africa) recorded by modern benthic foraminifera and their stable carbon isotopic composition. Deep-Sea Research Part I 53 (8), 1379–1405.

Eberwein, A., Mackensen, A., 2008. Last Glacial Maximum paleoproductivity and water masses off NW-Africa: evidence from benthic foraminifera and stable isotopes. Marine Micropaleontology 67, 87–103.

Eide, M., Olsen, A., Ninnemann, U.S., Johannessen, T., 2017. A global ocean climatology of preindustrial and modern ocean δ13C. Global Biogeochemical Cycles 31, 515–534.

Eisele, M., Hebbeln, D., Wienberg, C., 2008. Growth history of a cold-water coral covered carbonate mound – Galway Mound, Porcupine Seabight. NE-Atlantic Mar. Geol. 253, 160–169.

Eisele, M., Frank, N., Wienberg, C., Hebbeln, D., López Correa, M., Douville, E., Freiwald, A., 2011. Productivity controlled cold-water coral growth periods during the last glacial off Mauritania. Marine Geology 280, 143–149.

Eynaud, F., Turon, J.L., Duprat, J., 2004. Comparison of the Holocene and Eemian palaeoenvironments in the South-Icelandic basin: dinoflagellate cysts as proxies for the North Atlantic surface circulation. Review of Paleobotany and Palynology 128, 55–79.

Eynaud F., Malaizé B., Zaragosi S., de Vernal A., Scourse, J., Pujol C., Cortijo, E., Grousset, F.E., Penaud A., Toucanne S., Turon J.L., Auffert, G., 2012. New constraints on European glacial freshwater releases to the North Atlantic Ocean. Geophysical Research Letters 39, Article number L15601.

Falardeau, J., de Vernal, A., Spielhagen, R.F., 2018. Paleoceanography of northeastern Fram Strait since the last glacial maximum: Palynological evidence of large amplitude changes. Quaternary Science Reviews 195, 133–152.

Fiúza, A.F.G., Hamann, M., Ambar, I., Del Rio, G.D., González, N., Cabanas, J.M., 1998. Water masses and their circulation off western Iberia during May 1993. Deep Sea Res. I 45, 1127–1160.

Flecha, S., Perez, F.F., Navarro, G., Ruiz, J., Olive, I., Rodriguez-Galvez, S., Costas, E., Huertas, I. E., 2012. Anthropogenic carbon inventory in the Gulf of Cadiz. J. Mar. Syst. 92, 67–75.

Fontanier, C., Mackensen, A., Jorissen, F.J., Anschutz, P., Licari, L., Griveaud, C., 2006. Seasonal and trophic impacts on stable oxygen and carbon isotopes in live benthic foraminifera from the Bay of Biscay. Marine Micropaleontology 58, 159–183.

Frank, N., Lutringer, A., Paterne, M., Blamart, D., Henriet, J.-P., van Rooij, D., van Weering, T.C.E., 2005. Deep-water corals of the northeastern Atlantic margin: carbonate mound evolution and upper intermediate water ventilation during the Holocene. In: Freiwald, A., Roberts, J.M. (Eds.), Cold-water Corals and Ecosystems. Springer, Heidelberg, pp. 113–133.

Frank, N., Ricard, E., Lutringer-Paque, A., van der Land, C., Colin, C., Blamart, D., Foubert, A., Van Rooij, D., Henriet, J.-P., de Haas, H., van Weering, T.C.E., 2009. The Holocene occurrence of cold-water corals in the NE Atlantic: implications for coral carbonate mound evolution. Mar. Geol. 266, 129–142.

Freiwald, A., Fosså, J.H., Grehan, A., Koslow, T., Roberts, J.M., 2004. Cold-water Coral Reefs. UNEP-WCMC, Biodiversity Series 22, Cambridge, UK, 84 pp.

Frihmat, Y.E., Hebbeln, D., Jaaidi, E.B., Mhammdi, N., 2015. Reconstruction of productivity signal and deep-water conditions in Moroccan Atlantic margin (~35°N) from the last glacial to the Holocene. Springerplus 4, 69.

Galbraith, E.D., Jaccard, S.L., 2015. Deglacial weakening of the oceanic soft tissue pump: global constraints from sedimentary nitrogen isotopes and oxygenation proxies. Quat. Sci. Rev. 109, 38–48.

Ganne A., Leroyer C., Penaud A., Mojtahid M., 2016. Present-day palynomorph deposits in an estuarine context: the case of the Loire Estuary. Journal of Sea Research 118, 35–51.

Garcia Lafuente, J., Ruiz, J., 2007. The Gulf of Cadiz pelagic ecosystem: A review. Progress in Oceanography 74, 228–251.

Garcia Lafuente, J., Delgado, J., Criado Aldeanueva, F., Bruno, M., Del Rio, J., Vargas, J.M., 2006. Water mass circulation on the continental shelf of the Gulf of Cadiz. Deep Sea Research II 53 (11–13), 1182–1197.

Gehlen, M., A. Mucci, B. Boudreau, 1999. Modelling the distribution of stable carbon isotopes in porewaters of deep-sea sediments. Geochimica et Cosmochimica Acta 63(18), 2763–2773.

González, C., Dupont, L.M., Mertens, K., Wefer, G., 2008. Reconstructing marine productivity of the Cariaco Basin during marine isotope stages 3 and 4 using organic-walled dinoflagellate cysts. Paleoceanography 23, Pa3215.

Gottschalk, J., Vazquez Riveiros, N., Waelbroeck, C., Skinner, L.C., Michel, E., Duplessy, J.-C., Hodell, D., Mackensen, A., 2016a. Carbon isotope offsets between species of the genus *Cibicides* (*Cibicidoides*) in the glacial sub-Antarctic Atlantic Ocean. Paleoceanography 31, 1583–1602.

Gottschalk, J., Skinner, L.C., Lippold, J., Vogel, H., Frank, N., Jaccard, S.L., Waelbroeck, C., 2016b. Biological and physical controls in the Southern Ocean on past millennial-scale atmospheric CO2 changes. Nat. Commun. 7, 1–11.

Gottschalk, J., Battaglia, G., Fischer, H., Frolicher, T., Jaccard, S.L., Jeltsch-Thömmes, A., Joos, F., Köhler, P., Meissner, K.J., Menviel, L., Nehrbass-Ahles, C., Schmitt, J., Schmittner, A., Skinner, L.C., Stocker, T.F., 2019. Mechanisms of millennial-scale atmospheric CO2 change in numerical model simulations. Quat. Sci. Rev. 220, 30–74.

Gottschalk, J., Skinner, L.C., Jaccard, S.L., Menviel, L., Nehrbass-Ahles, C., Waelbroeck, C., 2020. Southern Ocean link between changes in atmospheric CO2 levels and northern-hemisphere climate anomalies during the last two glacial periods. Quat. Sci. Rev. 230 (106067).

Guiot, J., de Vernal, A., 2007. Tranfer functions: methods for quantitative paleoceanography based on microfossils. In: Hillaire-Marcel, de Vernal (Eds.), Proxies in Late Cenozoic Paleoceanography. Elsevier, pp. 523–563.

Habgood, E.L., Kenyon, N.H., Masson, D.G., Akhmetzhanov, A., Weaver, P.P.E., Gardner, J., Mulder, T., 2003. Deep-water sediment wave fields, bottom current sand channels and gravity flow channellobe systems: Gulf of Cadiz, NE Atlantic. Sedimentology 50, 483–510.

Hagen, E., 2001. Northwest African upwelling scenario. Oceanologica Acta 24, 113–128.

Hain, M.P., Sigman, D.M., Haug, G.H., 2010. Carbon dioxide effects of Antarctic stratification, North Atlantic Intermediate Water formation, and subantarctic nutrient drawdown during the last ice age: diagnosis and synthesis in a geochemical box model. Global Biogeochem. Cycles 24 (GB4023), 1–19.

Hammer, Ø., Harper, D.A.T., Ryan, P.D., 2001. Past: paleontological statistics software package for education and data analysis. Palaeontol. Electron. 4 (1), art. 4: 9pp., 178kb, http://palaeo-electronica.org/2001_1/past/issue1_01.htm.

Hardy, W., Penaud, A., Marret, F., Bayon, G., Marsset, T., Droz, L., 2016. Dinocyst assemblage constraints on oceanographic and atmospheric processes in the eastern equatorial Atlantic over the last 44 kyr. Biogeosciences 13, 4823–4841.

Hardy W., Marret F., Penaud A., Le Mézo P., Droz L., Marsset T., Kageyama M., 2018. Quantification of last glacial-Holocene net primary productivity and upwelling activity in the equatorial eastern Atlantic with a revised modern dinocyst database. Palaeogeography Palaeoclimatology Palaeoecology 505, 410–427.

Hoogakker, B.A.A., Elderfield, H., Schmiedl, G., McCave, I.N., Rickaby, R.E.M., 2015. Glacial-interglacial changes in bottom-water oxygen content on the Portuguese margin. Nat. Geosci. 8, 40–43.

Huertas, I.E., Navarro, G., Rodriguez-Galvez, S., Lubian, L.M., 2006. Temporal patterns of carbon dioxide in relation to hydrological conditions and primary production in the northeastern shelf of the Gulf of Cadiz (SW Spain). Deep-Sea Research II 53, 1344–1362.

Huertas, I. E., Rios, A.F., Garcia-Lafuente, J., Makaoui, A., Rodriguez-Galvez, S., Sanchez-Roman, A., Orbi, A., Ruiz, J., Perez, F.F., 2009. Anthropogenic and natural CO2 exchange through the Strait of Gibraltar. Biogeosciences 6, 647–662.

Jansen, M.F., 2017. Glacial ocean circulation and stratification explained by reduced atmospheric temperature. PNAS 114 (1), 45–50.

Kim, S.-Y., Scourse, J., Marret, F., Lim, D.-I., 2010. A 26,000-year integrated record of marine and terrestrial environmental change off Gabon, west equatorial Africa, Palaeogeogr. Palaeoclimatol., 297, 428–438.

Kucera, M., Weinelt, M., Kiefer, T., Pflaumann, U., Hayes, A., Weinelt, M., Chen, M.-T., Mix, A.C., Barrows, T.T., Cortijo, E., Duprat, J., Juggins, S., Waelbroeck, C., 2005. Reconstruction of sea-surface temperatures from assemblages of planktonic foraminifera: Multi-technique approach based on geographically constrained calibration data sets and its application to glacial Atlantic and Pacific Oceans. Quaternary Science Reviews 24 (7–9), 951–998. SPEC. ISS.

Lewis, J., Dodge, J.D., Powell, A.J., 1990. Quaternary dinoflagellate cysts from the upwelling system offshore Peru, hole 686B, ODP Leg 112. Proc. ODP Sci. Results 112, 323–327.

Limoges, A., Londeix, L., de Vernal, A., 2013. Organic-walled dinoflagellate cyst distribution in the Gulf of Mexico. Mar. Micropaleontol. 102, 51–68.

Lougheed, B. C., Obrochta, S.A., 2019. Rapid, Deterministic Age-Depth Modeling Routine for Geological Sequences With Inherent Depth Uncertainty. Paleoceanography and Paleoclimatology 34, 122–133.

Lynch-Stieglitz, J., Stocker, T., Broecker, W.S., Fairbanks, R.G., 1995. The influence of air-sea exchange on the isotopic composition of oceanic carbon: Observations and modeling. Global Biogeochemical Cycles 9, 653–665.

Mackensen, A., Licari, L., 2003. Carbon isotopes of live benthic foraminifera from the South Atlantic: sensitivity to bottom water carbonate saturation state and organic matter rain rates. In The South Atlantic in the Late Quaternary. Springer, Berlin, Heidelberg, pp. 623–644.

Marinov, I., Gnanadesikan, A., Toggweiler, J.R., Sarmiento, J.L., 2006. The Southern Ocean biogeochemical divide. Nature 441, 964–967.

Marret, F. and Turon, J. L., 1994. Paleohydrology and paleoclimatology off Northwest Africa during the last glacial-interglacial transition and the Holocene: Palynological evidences, Mar. Geol., 118, 107–117.

Marret, F., Zonneveld, K.A.F., 2003. Atlas of modern organic-walled dinoflagellate cyst distribution. Review of Palaeobotany and Palynology 125, 1–200.

Marret, F., Scourse, J., Kennedy, H., Ufkes, E., Jansen, J.F., 2008. Marine production in the Congo influenced SE Atlantic over the past 30,000 years: a novel dinoflagellate cyst based transfer function approach. Mar. Micropaleontol. 68, 198–222.

Marshall N.R., de Vernal A., Mucci A., Kienast M., Filippova A., Hillaire-Marcel C., 2021. Carbonate dissolution and environmental parameters govern coccolith vs. alkenone abundances in surface sediments from the northwest North Atlantic. Marine Micropaleontology 169, 102032.

McCorkle, D.C., Emerson, S.R., 1988. The relationship between pore water carbon isotopic composition and bottom water oxygen concentration. Geochim. Cosmochim. Acta 52, 1169–1178.

McCorkle, D.C., Keigwin, L.D., Corliss, B.H., Emerson, S.R., 1990. The influence of microhabitats on the carbon isotopic composition of deep-sea benthic foraminifera. Paleoceanography 5, 161–185.

McKay, C.L., Filipsson, H.L., Romero, O.E., Stuut, J.-B.W., Donner, B., 2014. Pelagicebenthic coupling within an upwelling system of the subtropical northeast Atlantic over the last 35 ka BP. Quaternary Science Reviews 106, 299–315.

Moreno, A., Cacho, I., Canals, M., Prins, M. A., Sánchez-Goñi, M. F., Grimalt, J. O., Weltje, G. J., 2002. Saharan dust transport and high-latitude glacial climatic variability: The Alboran Sea record, Quaternary Res., 58, 318–328.

Morzadec-Kerfourn, M.-T., 1977. Les kystes de Dinoflagellés dans les sédiments récents le long des côtes bretonnes. Rev. Micropaleontol. 20, 157–166.

Müller, P.J., Kirst, G., Ruhland, G., von Storch, I., Rosell-Melé, A., 1998. Calibration of the alkenone paleotemperature index U37K′ based on core-tops from the eastern South Atlantic and the global ocean (60°N–60°S). Geochim. Cosmochim. Acta 62, 1757–1772.

Navarro, G., Ruiz, J., 2006. Spatial and temporal variability of phytoplankton in the Gulf of Cadiz through remote sensing images. Deep-Sea Res. II Top. Stud. Oceanogr. 53, 1241–1260.

Navarro, G., Caballero, I., Prieto, L., Vázquez, A., Flecha, S. et al., 2012. Seasonal-to-interannual variability of chlo- Seasonal-to-interannual variability of chlorophyll-a bloom timing associated with physical forcing in the Gulf of Cadiz. Advances in Space Research 50 (8), 1164–1172.

Patton, G. M., Martin, P. A., Voelker, A., Salgueiro, E., 2011. Multiproxy comparison of oceanographic temperature during Heinrich Events in the eastern subtropical Atlantic, Earth Planet. Sc. Lett., 310, 45–58.

Peliz, A., Dubert, J., Santos, A., Oliveira, P., Le Cann, B., 2005. Winter upper ocean circulation in the Western Iberian Basin-Fronts, eddies and poleward flows: An overview. Deep Sea Res. I 52, 621–646.

Penaud A., Eynaud F., Turon J.L., Blamart D., Rossignol L., Marret F., Lopez-Martinez C., Grimalt J.O., Malaizé B., Charlier K., 2010. Contrasting paleoceanographic conditions off Morocco during Heinrich events (1 and 2) and the Last Glacial Maximum. Quaternary Science Reviews 29, 1923–1939.

Penaud A., Eynaud F., Voelker A., Kageyama, M., Marret F., Turon J.L., Blamart D., Mulder T., Rossignol L., 2011. Assessment of sea surface temperature changes in the Gulf of Cadiz during the last 30 ka: implications for glacial changes in the regional hydrography. Biogeosciences 8, 2295–2316.

Penaud, A., Eynaud, F., Voelker, A.H.L., Turon, J-L., 2016. Palaeohydrological changes over the last 50 ky in the central Gulf of Cadiz: complex forcing mechanisms mixing multi-scale processes. Biogeosciences, 13, 5357–5377.

Penaud, A., Ganne A., Eynaud F., Lambert C., Coste P.O., Herlédan M., Vidal M., Goslin J., Stéphan P., Charria G., Pailler Y., Durand M., Zumaque J., Mojtahid M., 2020. Oceanic versus continental influences over the last 7 kyrs from a midshelf record in the northern Bay of Biscay (NE Atlantic). Quaternary Science Reviews 229, 106–135.

Prahl, F.G., Wakeham, S.G., 1987. Calibration of unsaturation patterns in long-chain ketone compositions for paleotemperature assessment. Nature 330, 367–369.

Prieto, L., Navarro, G., Rodríguez-Gálvez, S., Huertas, I.E., Naranjo, J. et al., 2009. Oceanographic and meteorological forcing of the pelagic ecosystem on the Gulf of Cadiz shelf (SW Iberian Peninsula). Continental Shelf Research 29 (17), 2122–2137.

Radi, T., de Vernal, A., 2004. Dinocyst distribution in surface sediments from the northeastern Pacific margin (40–60°N) in relation to hydrographic conditions, productivity and upwelling. Rev. Palaeobot. Palynol. 128, 169–193.

Radi, T., de Vernal, A., 2008. Dinocysts as proxy of primary productivity in mid–high latitudes of the Northern Hemisphere. Mar. Micropaleontol. 68, 84–114.

Rasmussen, S. O., et al., 2014. A stratigraphic framework for abrupt climatic changes during the Last Glacial period based on three synchronized Greenland ice-core records: refning and extending the INTIMATE event stratigraphy. Quaternary Science Reviews 106, 14–28.

Rogerson, M., Schönfeld, J., Leng, M.J., 2011. Qualitative and quantitative approaches in palaeohydrography: A case study from core-top parameters in the Gulf of Cadiz. Marine Geology 280 (1–4), 150–167.

Rüggeberg, A., Dullo, W.-C., Dorschel, B., Hebbeln, D., 2007. Environmental changes and growth history of a cold-water carbonate mound (Propeller Mound, Porcupine Seabight). Int. J. Earth Sci. 96, 57–72.

Salgueiro, E., Voelker, A. H. L., de Abreu, L., Abrantes, F., Meggers, H., Wefer, G., 2010. Temperature and productivity changes off the western Iberian margin during the last 150 ky, Quaternary Sci. Rev., 29, 680–695.

Salgueiro, E., Naughton, F., Voelker, A. H. L., de Abreu, L., Alberto, A., Rossignol, L., Duprat, J., Magalhães, V. H., Vaqueiro, S., Turon, J. L., Abrantes, F., 2014. Past circulation along the western Iberian margin: a time slice vision from the Last Glacial to the Holocene, Quaternary Sci. Rev., 106, 316–329.

Sarmiento, J.L., Toggweiler, J.R., 1984. A new model for the role of the oceans in determining atmospheric pCO2. Nature 308, 621–624.

Schmittner, A., Somes, C.J., 2016. Complementary constraints from carbon (13C) and nitrogen (15N) isotopes on the glacial ocean's soft-tissue biological pump, Paleoceanography, 31, 669–693.

Schmittner, A., Bostock, H.C., Cartapanis, O., Curry, W.B., Filipsson, H.L., Galbraith, E.D., Gottschalk, J., Herguera, J.C., Hoogakker, B., Jaccard, S.L., Lisiecki, L.E., Lund, D.C., Martínez-Méndez, G., Lynch-Stieglitz, J., Mackensen, A., Michel, E., Mix, A.C., Oppo, D.W., Peterson, C.D., Repschläger, J., Sikes, E.L., Spero, H.J., Waelbroeck, C., 2017. Calibration of the carbon isotope composition (δ13C) of benthic foraminifera. Paleoceanography 32, 512–530.

Seierstad, I.K., P.M. Abbott, M. Bigler, T. Blunier, A.J. Bourne, E. Brook, S.L. Buchardt, C. Buizert, H.B. Clausen, E. Cook, 2014. Consistently dated records from the Greenland GRIP, GISP2 and NGRIP ice cores for the past 104 ka reveal regional millennial-scale δ18O gradients with possible Heinrich event imprint. Quaternary Science Reviews 106, 29-46.

Shi, N., Dupont, L. M., Beug, H.-J., Schneider, R., 1998. Vegetation and climate changes during the last 21 000 years in S.W. Africa based on a marine pollen record, Veget Hist Archaebot, 7, 127–140.

Targarona, J., Warnaar, J., Boessenkool, K.P., Brinkhuis, H., Canals, M., 1999. Recent dinoflagellate cyst distribution in the North Canary Basin, NW Africa. Grana 38, 170–178.

Umling, N.E., Thunell, R.C., 2017. Synchronous deglacial thermocline and deepwater ventilation in the eastern equatorial Pacific. Nat. Commun. 8 (14203), 1–10.

Umling, N.E., Thunell, R.C., 2018. Mid-depth respired carbon storage and oxygenation of the eastern equatorial Pacific over the last 25,000 years. Quaternary Science Reviews 189, 43–56.

Van der Bilt, W.G.M. Lane, C.S., 2019. Lake sediments with Azorean tephra reveal ice-free conditions on coastal northwest Spitsbergen during the Last Glacial Maximum. Sci. Adv. 5, eaaw5980.

Voelker, A.H., Lebreiro, S., Schönfeld, J., Cacho, I., Erlenkeuser, H., Abrantes, F., 2006. Mediterranean outflow strengthening during northern hemisphere coolings: a salt source for the glacial Atlantic? Earth and Planetary Science Letters 245, 39–55.

Waelbroeck, C., Labeyrie, L., Michel, E., Duplessy, J.C., McManus, J.F., Lambeck, K., Balbon, E., Labracherie, M., 2002. Sea-level and deep water temperature changes derived from benthic foraminifera isotopic records. Quaternary Science Reviews 21 (1-3), 295–305.

Waelbroeck C., Lougheed B.C., Vazquez Riveiros N., Missiaen L., Pedro J., Dokken T., Hajdas I., Wacker L., Abbott P., Dumoulin J.-P., Thil F., Eynaud F., Rossignol L., Fersi W., Albuquerque A.L., Arz H., Austin W., Came R., Carlson A., Collins J., Dennielou B., Desprat S., Dickson A., Elliot M., Farmer C., Giraudeau J., Gottschalk J., Henderiks J., Hughen K., Jung S., Knutz P., Lebreiro S., Lund D., Lynch-Stieglitz J., Malaizé B., Marchitto T., Martinez Mendez G., Mollenhauer G., Naughton F., Nave S., Nünberg D., Oppo D., Peck V., Penaud A., Portilho Ramos R., Repschläger J., Roberts J., Rühlemann C., Salgueiro E., Sanchez Goni M., Schönfeld J., Scussolini P., Skonieczny C., Thornalley D., Toucanne S., Van Rooij D., Vidal L., Voelker A., Wary M., Weldeab S., Ziegler M., 2019. Consistently dated Atlantic sediment cores over the last 40 thousand years. Scientific Data 165.

Wan, S., Clift, P.D., Zhao, D., Hovius, N., Munhoven, G., France-Lanord, C., Wang, Y., Xiong, Z., Huang, J., Yu, Z., Zhang, J., Ma, W., Zhang, G., Li, A., Li, T., 2017. Enhanced silicate weathering of tropical shelf sediments exposed during glacial lowstands: A sink for atmospheric CO2. Geochimica et Cosmochimica Acta 200, 123–144.

Wary M., Eynaud F., Rossignol L., Zaragosi S., Sabine M., Castera M.H., Billy I., 2017. The southern Norwegian Sea during the last 45 ka: hydrographical reorganizations under changing ice-sheet dynamics, Journal of Quaternary Science, 32, 908–922.

Wienberg, C., Hebbeln, D., Fink, H.G., Mienis, F., Dorschel, B., Vertino, A., López Correa, M., Freiwald, A., 2009. Scleractinian cold-water corals in the Gulf of Cádiz – first clues about their spatial and temporal distribution. Deep Sea Res. I 56, 1873–1893.

Wienberg, C., Frank, N., Mertens, K.N., Stuut, J.B., Marchant, M., Fietzke, J., Mienis, F., and Hebbeln, D., 2010. Glacial cold-water coral growth in the Gulf of Cádiz: Implications of increased palaeo-productivity: Earth and Planetary Science Letters. 298, 405–416.

Wooster, W.S., Bakun, A., McLain, D.R., 1976. The seasonal upwelling cycle along the eastern boundary of the North Atlantic. Journal of Marine Research 34, 131–141.

Zahn, R., Winn, K., Sarnthein, M., 1986. Benthic foraminiferal $\delta^{13}C$ and accumulation rates of organic carbon: *Uvigerina peregrina* group and *Cibicidoides wuellerstorfi*. Paleoceanography 1, 27–42.

Zonneveld, K.A.F., Hoek, R., Brinkhuis, H., Willems, H., 2001. Lateral distribution of organic walled dinoflagellates in surface sediments of the Benguela upwelling Region. Prog. Oceanogr. 48, 25–72.

Zonneveld, K.A.F., Marret, F., Versteegh, G.J.M., Bogus, K., Bonnet, S., Bouimetarhan, I., Crouch, E., de Vernal, A., Elshanawany, R., Edwards, L., Esper, O., Forke, S., Grøsfjeld, K., Henry, M., Holzwarth, U., Kielt, J.-F., Kim, S.-Y., Ladouceur, S., Ledu, D., Chen, L., Limoges, A., Londeix, L., Lu, S.-H., Mahmoud, M.S., Marino, G., Matsouka, K., Matthiessen, J., Mildenhal, D.C., Mudie, P., Neil, H.L., Pospelova, V., Qi, Y., Radi, T., Richerol, T., Rochon, A., Sangiorgi, F., Solignac, S., Turon, J.-L., Verleye, T., Wang, Y., Wang, Z., Young, M., 2013. Atlas of modern dinoflagellate cyst distribution based on 2405 data points. In: Review of Palaeobotany and Palynology, Atlas of Modern Dinoflagellate Cyst Distribution Based on 2405 Data Points. 191. pp. 1–197.